Computationally Efficient Carrier Integer Ambiguity Resolution in Multiepoch GPS/INS: A Common-Position-Shift Approach

Yiming Chen, *Member, IEEE*, Sheng Zhao, and Jay A. Farrell, *Fellow, IEEE*

***Abstract*— Integer ambiguity resolution is a challenging technical issue that exists in real-time kinematic (RTK) global positioning system (GPS) navigation. Once the integer vector is resolved, centimeter-level positioning estimation accuracy can be achieved using the GPS carrier phase measurements. Recently, a real-time sliding window Bayesian estimation approach to RTK GPS and inertial navigation was proposed to provide reliable centimeter accurate-state estimation, via integer ambiguity resolution utilizing a prior along with all inertial measurement unit and GPS measurements within the time window. One challenge to implementing that approach in practice is the high computation cost. This paper proposes a novel implementation approach with significantly lower computational requirements and includes a thorough theoretical analysis. The implementation results show that the proposed method resolves an integer vector identical to that of the original method and achieves state estimation with centimeter global positioning accuracy.**

***Index Terms*— Global positioning system (GPS), inertial navigation, inertial navigation system (INS), integer ambiguity, real-time kinematic (RTK), sliding window estimation.**

I. Introduction

INTEGRATION of GPS and aided inertial navigation system (INS) has proven useful due to their complementary nature [1]. The INS provides a continuous high-bandwidth state vector estimate. GPS aiding corrects errors accumulated by the integrative INS process and calibrates the inertial measurement unit (IMU). The overall accuracy of GPS aided INS depends on the accuracy, frequency, and reliability of the GPS measurements. A well-designed GPS receiver can typically reach a stand-alone positioning accuracy of 3–8 m [2]. To reliably achieve higher accuracy positioning, differential GPS (DGPS) is required. With a base station within a range of a few tens of kilometers, DGPS accuracy is on the order of 1 m, growing at the rate of 1 m per 150 km of separation [3]. A user can either set up a base station on their own or utilize publicly available correction services: Continuously Operating Reference Station (CORS) [4], nationwide DGPS [5], and European Geodetic Reference Systems [6]. As mobile communication networks (4G or Wi-Fi) become available, DGPS techniques will become ubiquitous. In this paper, all GPS measurements are assumed to be processed differentially.

GPS receivers provide carrier phase measurements that are biased by an unknown integer number of wavelengths. While the phase-locked loop (PLL) of a receiver channel maintains phase lock, the unknown integer for the satellite being tracked remains constant. When loss of lock eventually happens (i.e., a cycle-slip occurs), the new integer is most likely to be different. The fundamental ideas underlying integer ambiguity resolution rely on reformulating the problem into an integer least squares (ILS) approach, e.g., LAMBDA [7], MLAMBDA [8], or MILES [9]. Real-time kinematic (RTK) applications solve the ILS and position estimation problems simultaneously in real time [10]–[12] and may involve multiple GPS epochs, but without IMU constraints between epochs. The solution of the RTK problem is simplified, yet still challenging when dual-frequency receivers are available, because the integers can be resolved by forming the wide-lane phase measurements [11]. When the integer vector can be resolved, centimeter positioning accuracy is achievable in real time on moving platforms [13]. The performance of the conventional single-epoch resolution is strongly influenced by the number of available satellites, the geometry of the received satellite constellation, and the quality of the measurements. If noisy or faulty measurements exist, the integer resolution can be wrong, without sufficient measurement redundancy to detect the error. For single-frequency receivers, integer ambiguity resolution is even more challenging due to the inability to form the wide-lane measurement and the smaller number (i.e., half) of measurements.

In [14], a contemplative real-time (CRT) approach was proposed to provide a reliable DGPS/INS solution. Within the CRT framework [14]–[19], the full nonlinear maximum *a posteriori* (MAP) estimation problem is solved considering all the information (e.g., prior, kinematics, GPS, and IMU sensor data) available within a multiepoch window [20]–[23]. The CRT approach provides a large enough set of residuals to

Manuscript received April 17, 2015; revised September 16, 2015; accepted October 30, 2015. Date of publication December 8, 2015; date of current version August 4, 2016. Manuscript received in final form November 10, 2015. This work was supported in part by a 2013/2014 University of California Transportation Center Dissertation Award and in part by the U.S. Army under Grant W911NF-12-1-0094. Recommended by Associate Editor A. Alessandri.

Y. Chen was with the Department of Electrical and Computer Engineering, University of California at Riverside, Riverside, CA 92521 USA. He is now with Qualcomm Research, San Diego, CA 92121 USA (e-mail: yichen@ee.ucr.edu).

S. Zhao was with the Department of Electrical and Computer Engineering, University of California at Riverside, Riverside, CA 92521 USA. He is now with Google, Mountain View, CA 94043 USA (e-mail: shzhao@ee.ucr.edu).

J. A. Farrell is with the Department of Electrical and Computer Engineering, University of California at Riverside, Riverside, CA 92521 USA (e-mail: farrell@ee.ucr.edu).

Color versions of one or more of the figures in this paper are available online at http://ieeexplore.ieee.org.

Digital Object Identifier 10.1109/TCST.2015.2501352

extend Receiver Autonomous Integrity Monitoring techniques [24], [25] to reduce the effects of the outlier measurements on the estimation and to detect incorrect integers. In [17], integer ambiguity resolution is considered within the CRT framework for the RTK GPS/INS application.

One challenge to implementing integer ambiguity resolution using GPS and IMU is the high computation load, especially when the multiepoch data window is long to enhance reliability or the IMU sampling rate is high. This paper considers an alternative solution with a significantly lower computational cost. The validity of the approach is demonstrated theoretically and the performance is demonstrated experimentally. The implementation results demonstrate that the proposed method can achieve centimeter-level position accuracy on moving platforms in challenging GPS environments and estimate integers identical to those from the original CRT method.

The outline of this paper is as follows. Section II states the RTK GPS/INS problem. Section III revisits the CRT integer ambiguity resolution proposed in [17]. Section IV presents the proposed *common-position-shift* (CPS) method. Section V analyzes the CPS method mathematically. Section VI presents the implementation results. Section VII concludes this paper.

II. Problem Statement

This section presents DGPS [26] and aided INS [1] background and notation.

A. Aided Inertial Navigation

Let $\boldsymbol{x} \in \mathbb{R}^{n_s}$ denote the rover state vector. For example, the state vector at time t

$$\boldsymbol{x}(t) = \left[\boldsymbol{p}^\mathsf{T}(t), \boldsymbol{v}^\mathsf{T}(t), \boldsymbol{q}^\mathsf{T}(t), \boldsymbol{b}_a^\mathsf{T}(t), \boldsymbol{b}_g^\mathsf{T}(t)\right]^\mathsf{T} \in \mathbb{R}^{n_s}$$

is composed of the position, velocity, attitude (e.g., quaternion), accelerometer bias, and gyroscope bias vectors.

The kinematic equations for the rover state are

$$\dot{\boldsymbol{x}}(t) = \boldsymbol{f}(\boldsymbol{x}(t), \boldsymbol{u}(t)) \tag{1}$$

where $\boldsymbol{f} : \mathbb{R}^{n_s} \times \mathbb{R}^6 \mapsto \mathbb{R}^{n_s}$ represents the kinematics and $\boldsymbol{u} \in \mathbb{R}^6$ is the vector of specific forces and angular rates. The function $\boldsymbol{f}$ is accurately known (see [1, Ch. 11]).

Given a distribution for the initial state $\boldsymbol{x}(t_1) \sim \mathcal{N}(\boldsymbol{x}_1, \mathbf{P}_1)$, where $\boldsymbol{x}_1 \in \mathbb{R}^{n_s}$ and $\mathbf{P}_1 \in \mathbb{R}^{n_s \times n_s}$, and measurements $\tilde{\boldsymbol{u}}$ of $\boldsymbol{u}$, the INS propagates the estimate of the rover state between aiding measurement time instants by solving

$$\dot{\hat{\boldsymbol{x}}}(t) = \boldsymbol{f}(\hat{\boldsymbol{x}}(t), \tilde{\boldsymbol{u}}(t)) \tag{2}$$

where $\hat{\boldsymbol{x}}(t)$ denotes the estimate of $\boldsymbol{x}(t)$.

For the convenience of later discussion, we define

$$\boldsymbol{s}(t) = \left[\boldsymbol{v}^\mathsf{T}(t), \boldsymbol{q}^\mathsf{T}(t), \boldsymbol{b}_a^\mathsf{T}(t), \boldsymbol{b}_g^\mathsf{T}(t)\right]^\mathsf{T} \in \mathbb{R}^{(n_s-3)} \tag{3}$$

as the state vector excluding the position. Then, we have $\boldsymbol{x}(t) = [\boldsymbol{p}^\mathsf{T}(t), \boldsymbol{s}^\mathsf{T}(t)]^\mathsf{T}$. Similarly, $\boldsymbol{x}_1 = [\boldsymbol{p}_1^\mathsf{T}, \boldsymbol{s}_1^\mathsf{T}]^\mathsf{T}$ for the prior and $\hat{\boldsymbol{x}}(t) = [\hat{\boldsymbol{p}}^\mathsf{T}(t), \hat{\boldsymbol{s}}^\mathsf{T}(t)]^\mathsf{T}$ for the state estimate.

Due to prior errors, system calibration errors, and measurement noise, the state estimation error $\delta\boldsymbol{x}(t) = \boldsymbol{x}(t) - \hat{\boldsymbol{x}}(t)$ develops over time. The dynamics and stochastic properties of this estimation error are derived from (1) and (2).

When aiding measurements

$$\tilde{\boldsymbol{z}}(t) = \boldsymbol{h}(\boldsymbol{x}(t)) + \boldsymbol{n}_z(t) \tag{4}$$

are available, various methods (e.g., the extended Kalman filter and particle filter) are available to use the initial state, inertial measurements, and aiding measurement information to estimate the rover state vector [1], [27].

B. DGPS Measurements

Throughout this paper, double-differenced GPS measurements are considered. For notational simplicity, it is assumed that the double-difference approach completely removes all common-mode errors (e.g., ionosphere, troposphere, satellite clock, and ephemeris) as well as the receiver clock biases, which allows these terms to be dropped throughout this paper. This is done only to simplify the notation of the presentation, and these errors will still affect the experimental results; therefore, outlier measurements may exist due to multipath error, heavy foliage, receiver failure, and so on.

The double-differenced pseudorange (i.e., code) measurement for the ith satellite are modeled as

$$\rho^i(t_k) = h_k^i(\boldsymbol{x}(t_k)) + n_\rho^i(t_k) \tag{5}$$

where $h_k^i(\boldsymbol{x}(t_k)) = \|\boldsymbol{p}(t_k) - \boldsymbol{p}^i(t_k)\|_2$ is the Euclidean distance at t_k between the rover position $\boldsymbol{p} \in \mathbb{R}^3$ and the position of the ith satellite $\boldsymbol{p}^i \in \mathbb{R}^3$, and $n_\rho^i \sim \mathcal{N}(0, \sigma_\rho^2)$ represents the (noncommon mode) measurement noise with standard deviation $\sigma_\rho = 0.5 \sim 3m$, depending on receiver design, environmental factors, and the performance of multipath mitigation techniques [28]. In practice, the noise level σ_ρ will vary temporally and spatially for each satellite.

The double-differenced carrier phase measurement for the ith satellite is modeled as

$$\varphi^i(t_k) = h_k^i(\boldsymbol{x}(t_k)) + \lambda N^i(t_k) + n_\varphi^i(t_k) \tag{6}$$

where λ is the carrier phase wavelength and N^i is the unknown integer ambiguity. The measurement noise has distribution $n_\varphi^i \sim \mathcal{N}(0, \sigma_\varphi^2)$. The noise standard deviation σ_φ is millimeter to centimeter level ($<0.01\sigma_\rho$).

The unknown integer N^i represents the number of carrier wave cycles between the satellite and the receiver at the time that phase lock is achieved. If the PLL in the receiver for the ith satellite maintains lock without cycle slips during a time interval $[t_1, t_n]$, then this integer is constant over this time interval, i.e., $N^i(t_1) = \cdots = N^i(t_n) = N^i$. The receiver reports the lock status to enable detection of such time intervals. The unknown integer must be estimated exactly to enable the use of the carrier phase measurement for precise position estimation. Note that the carrier phase measurement model does not match the standard measurement model in (4), because there is an unknown integer variable N^i.

C. Technical Problem Statement

This paper investigates integer ambiguity resolution and trajectory estimation over a time interval $[t_1, t_K]$ that we will

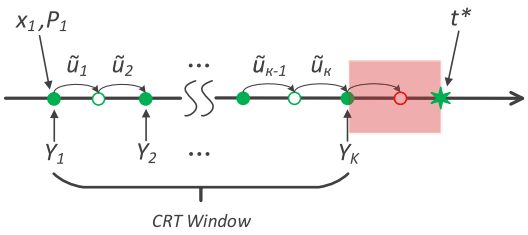

Fig. 1. Illustration of the CRT window measurement timeline. The window contains a prior for the initial state, K GPS measurements, and many IMU measurements between each pair of GPS measurements. IMU measurement times are indicated as dots on the timeline. All of these items yield constraints on the estimated trajectory $\hat{\boldsymbol{X}}$ during the CRT window.

refer to as the *CRT window*. This window contains K GPS measurement epochs, where K can be designer specified, time varying, or data dependent. A typical but simplified measurement scenario is shown in Fig. 1. The dots on the timeline indicate IMU measurement times τ_n. Typically, the number of IMU measurements between GPS measurements is very high (i.e., $t_{i+1} - t_i \gg \tau_{j+1} - \tau_j$). This is because the IMU sample frequency (e.g., 200 Hz) is at least twice the IMU bandwidth (e.g., 60 Hz), which is higher than the vehicle motion bandwidth (e.g., 10 Hz). The GPS sample rate is usually much lower (e.g., 1.0 Hz). The state transition between these times is constrained by the kinematic model of (2) and the IMU data. Additional constraints are imposed by the initial estimate $(\boldsymbol{x}_1, \mathbf{P}_1)$ depicted above the initial state and GPS measurements depicted below the timeline. Each of these constraints is quantified by a probability density that enables a Bayesian estimation formulation for the CRT estimation problem. The computation for the CRT estimation process considering all the information over the CRT window starts at t_K and completes its computation at $t^* = t_K + \Delta_K$, where $\Delta_K > 0$ is a small fraction of a second using standard off-the-shelf computers. The time interval (t_K, t^*) is shown in Fig. 1 marked in red. For $t \in (t_K, t^*)$, the real-time state estimate is maintained by the INS. At t^*, the CRT estimation result $\hat{\boldsymbol{x}}(t_K)$ is propagated by the INS with the IMU data over $(t_K, t^*]$ and used to update the real-time estimate. Therefore, the INS is effectively free integrating without corrections, from $t_{K-1} + \Delta_{K-1}$ to $t_K + \Delta_K$, which is about 1 s, as in the standard EKF approach. For 1-Hz GPS epochs, the INS error accumulation is at the centimeter level.

To simplify the presentation of the novel ideas in this paper, the following assumptions are made.

Assumption 1: Within the CRT window, the receiver provides valid carrier phase measurements for m satellites, without loss of lock. △

Assumption 2: The prior distribution for $\boldsymbol{s}(t_1)$ is $N(\boldsymbol{s}_1, \mathbf{P}_{s_1})$. △

Assumption 3: The GPS measurement rate is 1 Hz. △

With Assumption 1, the unknown integers in the carrier phase measurements from these m satellites are constants over $[t_1, t_K]$. This assumption will be relaxed in the example section. Assumption 2 allows the system to be initialized at an unknown location, while the partial state estimate $\hat{\boldsymbol{s}}(t_1)$ is initialized with the prior $(\boldsymbol{s}_1, \mathbf{P}_{s_1})$ based on other information sources, while the position is estimated in the CRT window based on GPS. The GPS sampling rate stated in Assumption 3 facilitates the presentation. The entire derivation goes through for other sample rates. Under Assumptions 1–3, the CRT estimation problem considered in this paper can be stated as follows.

For a system described by (1), we have the following.

1) An initial distribution for the state $\boldsymbol{s}(t_1) \sim \mathcal{N}(\boldsymbol{s}_1, \mathbf{P}_{s_1})$.
2) IMU measurements $\mathbf{U} = \{\mathbf{U}_k\}_{k=1}^{K-1}$, where

$$\mathbf{U}_k = \{\tilde{\boldsymbol{u}}(\tau_n), t_k \le \tau_n \le t_{k+1}\}.$$

3) DGPS code and carrier phase measurements $\mathbf{Y} = \{\mathbf{Y}_k\}_{k=1}^{K}$, where

$$\mathbf{Y}_k = \{\rho^i(t_k)\}_{i=1}^{m_k} \bigcup \{\varphi^i(t_k)\}_{i=1}^{m}.$$

Note that $t_1, \ldots, t_k \in (\tau_1, \tau_\kappa]$. The set $\{\tau_n\}_{n=1}^{\kappa}$ contains the high-frequency IMU measurement time instants. The integer m_k is the total number of valid pseudorange measurements at time t_k. For simplicity of discussion in this paper, it is assumed that $m_k \equiv m$. The method presented in this paper can be extended to more complicated mixes of measurements.

Then, the objective is as follows.

Objective 1: Estimate the optimal state trajectory $\mathbf{X} \triangleq [\boldsymbol{x}^\intercal(t_1), \ldots, \boldsymbol{x}^\intercal(t_K)]^\intercal \in \mathbb{R}^{Kn_s}$ and integers $\mathbf{N} \triangleq [N^1, \ldots, N^m]^\intercal \in \mathbb{Z}^m$ with the given sensor measurements $\mathbf{U}$ and $\mathbf{Y}$, and the prior state density $p_{\boldsymbol{s}}(\boldsymbol{s}(t_1))$. △

In [17], the above objective is achieved by formulating and solving the corresponding MAP estimation problem. The accuracy and reliability of the solution is achieved by the nonlinear mixed ILS (MILS) method and faulty data removal scheme. This CRT integer ambiguity resolution method is revisited in Section III to make this paper self-contained.

III. CRT Integer Ambiguity Resolution

Let $\mathbf{X}_+ \triangleq \{\boldsymbol{x}(t) \text{ for } t = t_2, \ldots, t_K\}$, then the joint probability $p(\mathbf{X}, \mathbf{N}, \mathbf{Y}, \mathbf{U})$ can be factored as

$$\begin{aligned} p(\mathbf{X}, \mathbf{N}, \mathbf{Y}, \mathbf{U}) &= p(\mathbf{X}, \mathbf{U}, \mathbf{N}) p(\mathbf{Y}|\mathbf{X}, \mathbf{U}, \mathbf{N}) \\ &= p(\mathbf{X}_+, \boldsymbol{x}(t_1), \mathbf{U}) p(\mathbf{Y}|\mathbf{X}, \mathbf{N}) \\ &= p(\boldsymbol{x}(t_1), \mathbf{U}) p(\mathbf{X}_+|\boldsymbol{x}(t_1), \mathbf{U}) p(\mathbf{Y}|\mathbf{X}, \mathbf{N}) \\ &= p(\boldsymbol{x}(t_1)) p(\mathbf{X}_+|\boldsymbol{x}(t_1), \mathbf{U}) p(\mathbf{Y}|\mathbf{X}, \mathbf{N}) \\ &= p(\boldsymbol{s}(t_1)) p(\mathbf{X}_+|\boldsymbol{x}(t_1), \mathbf{U}) p(\mathbf{Y}|\mathbf{X}, \mathbf{N}). \end{aligned} \quad (7)$$

For a given prior $(\boldsymbol{s}_1, \mathbf{P}_{s_1})$ and data sets $\mathbf{Y}$ and $\mathbf{U}$, the MAP trajectory estimate is the $\mathbf{X}$ and $\mathbf{N}$ maximizing the right-hand side of (7)

$$\max_{\mathbf{X} \in \mathbb{R}^{n_s K}, \mathbf{N} \in \mathbb{Z}^m} p(\boldsymbol{s}(t_1)) p(\mathbf{X}_+|\boldsymbol{x}(t_1), \mathbf{U}) p(\mathbf{Y}|\mathbf{X}, \mathbf{N}). \quad (8)$$

With a Gaussian noise assumption, the negative log-likelihood of the right-hand side of (7) is

$$\begin{aligned}\|\mathbf{v}(\mathbf{X},\mathbf{N})\|^2_{\mathbf{W}} &= \|\boldsymbol{s}(t_1)-\boldsymbol{s}_1\|^2_{\mathbf{P}_{s_1}} \\ &+\sum_k \|\boldsymbol{\phi}(\boldsymbol{x}(t_k),\mathbf{U}_k)-\boldsymbol{x}(t_{k+1})\|^2_{\mathbf{Q}_k} \\ &+\sum_k\sum_i \left\|h^i_k(\boldsymbol{x}(t_k))-\rho^i(t_k)\right\|^2_{\sigma^2_\rho} \\ &+\sum_k\sum_i \left\|h^i_k(\boldsymbol{x}(t_k))+\lambda N^i-\varphi^i(t_k)\right\|^2_{\sigma^2_\varphi} \quad (9)\end{aligned}$$

where $\|\mathbf{v}\|^2_{\mathbf{W}}=\mathbf{v}^\top\mathbf{W}^{-1}\mathbf{v}$ is the squared Mahalanobis distance with matrix $\mathbf{W}$. All terms on the right-hand side also use this notation. The vector $\mathbf{v}$ is the concatenation of each of the vectors summed in the right-hand side of (9). The operator $\boldsymbol{\phi}$ and the covariance matrix $\mathbf{Q}_k$ used in (9) are defined in Appendix I. The matrix $\mathbf{W}$ is the positive definite block diagonal matrix formed by the positive definite submatrices $\mathbf{Q}_k$, $\mathbf{P}_{s_1}$, $\sigma^2_\rho\mathbf{I}$, and $\sigma^2_\varphi\mathbf{I}$. Using MATLAB syntax, $\mathbf{W}$ can be represented as $\mathbf{W}=\text{blkdiag}\big(\mathbf{P}_{s_1},\mathbf{Q}_0,\ldots,\mathbf{Q}_{K-1},\sigma^2_\rho\mathbf{I},\sigma^2_\varphi\mathbf{I}\big)$. Let $\Sigma_W{}^\intercal\Sigma_W=\mathbf{W}^{-1}$, then

$$\boldsymbol{r}\triangleq\Sigma_W\mathbf{v} \quad (10)$$

is the weighted residual and $\|\mathbf{v}\|^2_{\mathbf{W}}=\|\boldsymbol{r}\|^2$. For notation simplicity, herein we denote the tuple $(\mathbf{X},\mathbf{N})=[\mathbf{X}^\intercal,\mathbf{N}^\intercal]^\intercal\in\mathbb{R}^{n_sK}\times\mathbb{Z}^m$. With this notation, the MAP problem is transformed into the nonlinear NMILS problem

$$(\mathbf{X}^*,\mathbf{N}^*)=\underset{\mathbf{X}\in\mathbb{R}^{n_sK},\mathbf{N}\in\mathbb{Z}^m}{\arg\min}\ \|\boldsymbol{r}(\mathbf{X},\mathbf{N})\|^2 \quad (11)$$

where $\boldsymbol{r}$ is the vector

$$\boldsymbol{r}(\mathbf{X},\mathbf{N})=\begin{bmatrix}\Sigma_{\mathbf{P}_{s_1}}(\boldsymbol{s}(t_1)-\boldsymbol{s}_1)\\ \hdashline \Sigma_{\mathbf{Q}_1}(\boldsymbol{\phi}(\boldsymbol{x}(t_1),\mathbf{U}_1)-\boldsymbol{x}(t_2))\\ \vdots\\ \Sigma_{\mathbf{Q}_{K-1}}(\boldsymbol{\phi}(\boldsymbol{x}(t_{K-1}),\mathbf{U}_{K-1})-\boldsymbol{x}(t_K))\\ \hdashline \sigma_\rho^{-1}\big(h^1_1(\boldsymbol{x}(t_1))-\rho^1(t_1)\big)\\ \vdots\\ \sigma_\rho^{-1}\big(h^m_K(\boldsymbol{x}(t_K))-\rho^m(t_K)\big)\\ \sigma_\varphi^{-1}\big(h^1_1(\boldsymbol{x}(t_1))+\lambda N^1-\varphi^1(t_K)\big)\\ \vdots\\ \sigma_\varphi^{-1}\big(h^m_K(\boldsymbol{x}(t_K))+\lambda N^m-\varphi^m(t_K)\big)\end{bmatrix}.$$

The dashed lines separate the residuals into three sets: prior, INS, and GPS. This is only to facilitate discussion in Remark 2.

The CRT integer ambiguity resolution and trajectory estimation approach from [17] can be summarized with the following three steps.

1) Obtain the *float solution* by neglecting the integral nature of the ambiguity $\mathbf{N}$

$$(\check{\mathbf{X}},\check{\mathbf{N}})=\underset{(\mathbf{X},\mathbf{N})\in\mathbb{R}^{n_sK+m}}{\arg\min}\ \|\boldsymbol{r}(\mathbf{X},\mathbf{N})\|^2. \quad (12)$$

   Standard outlier rejection techniques [14], [25], [29], [30] can be executed to detect and remove outliers.
2) Starting from $(\check{\mathbf{X}},\check{\mathbf{N}})$, solve the NMILS problem in (11) to obtain the optimal solution $(\mathbf{X}^*,\mathbf{N}^*)$.
3) Check the validity of integer estimates with integer validation techniques [31].

The second step of this approach is computationally expensive, especially with relinearization, which requires reintegration. An alternative to the second step is the main focus herein.

To solve the optimization in (11) in an iterative manner, the *residual* $\boldsymbol{r}(\mathbf{X},\mathbf{N})$ is linearized around the current estimates $(\hat{\mathbf{X}},\hat{\mathbf{N}})$

$$\boldsymbol{r}(\mathbf{X},\mathbf{N})\approx\boldsymbol{r}(\hat{\mathbf{X}},\hat{\mathbf{N}})+\mathbf{J}(\hat{\mathbf{X}},\hat{\mathbf{N}})(\delta\mathbf{X},\delta\mathbf{N}) \quad (13)$$

where $\mathbf{J}(\hat{\mathbf{X}},\hat{\mathbf{N}})$ is the Jacobian matrix of $\boldsymbol{r}(\mathbf{X},\mathbf{N})$ evaluated at $(\hat{\mathbf{X}},\hat{\mathbf{N}})$ and $(\delta\mathbf{X},\delta\mathbf{N})=(\mathbf{X},\mathbf{N})-(\hat{\mathbf{X}},\hat{\mathbf{N}})$ is the estimation error. Furthermore, $\mathbf{J}(\hat{\mathbf{X}},\hat{\mathbf{N}})$ can be decomposed as

$$\mathbf{J}(\hat{\mathbf{X}},\hat{\mathbf{N}})=[\mathbf{A},\mathbf{B}]$$

where $\mathbf{A}$ contains the columns of $\mathbf{J}(\hat{\mathbf{X}},\hat{\mathbf{N}})$ that are partial with respect to $\mathbf{X}$ and $\mathbf{B}$ contains the partial with respect to $\mathbf{N}$. Thus, (13) can be rewritten as

$$\boldsymbol{r}(\mathbf{X},\mathbf{N})\approx\boldsymbol{r}(\hat{\mathbf{X}},\hat{\mathbf{N}})+\mathbf{A}\delta\mathbf{X}+\mathbf{B}\delta\mathbf{N}.$$

The next step solves the MILS problem

$$\min_{\delta\mathbf{X}\in\mathbb{R}^{n_sK},\delta\mathbf{N}\in\mathbb{Z}^m}\|\boldsymbol{r}(\hat{\mathbf{X}},\hat{\mathbf{N}})+\mathbf{A}\delta\mathbf{X}+\mathbf{B}\delta\mathbf{N}\|^2. \quad (14)$$

Solution methods are well presented in [7]–[9] and [32]–[34]. Any of these methods could be used to solve the MILS problem embedded in Step 2) of the problem of interest. For the presentation of this paper, we choose to use MILES framework [9] for both the presentation and solution. The CPS algorithm could also be implemented using LAMBDA [7] and MLAMBDA [8]. The performance is expected to be similar.

Remark 1: Note that the major contribution of this paper is not a method for MILS solution; instead, it is to present an innovative way to reconstruct the cost function in (9) into two parts that can be solved independently and efficiently. △

Remark 2: Note that the vector defining $\boldsymbol{r}(\mathbf{X},\mathbf{N})$ is divided by horizontal lines into three parts. Standard multiepoch RTK would only address the residuals in the bottom portion of the vector. The residuals from that portion of the vector come from nonlinearities (i.e., range measurements) with a very small curvature [i.e., $1/(20\times10^6)$ m] so that the problem is essentially linear and a single MILS iteration is sufficient. The method herein also considers the prior and the IMU constraints. Many important applications contain an IMU to attain a high-frequency and high-bandwidth state vector estimate. The nonlinearities in the INS are strong, having curvature that is significant relative to the state uncertainty, especially at startup or during maneuvers; therefore, multiple iterations of the MILS may be required. △

By dropping the notation $(\hat{\mathbf{X}},\hat{\mathbf{N}})$ in $\boldsymbol{r}(\hat{\mathbf{X}},\hat{\mathbf{N}})$ and defining the **QR** decomposition [46]

$$\mathbf{A}=[\mathbf{Q}_A,\bar{\mathbf{Q}}_A]\begin{bmatrix}\mathbf{R}_A\\ \mathbf{0}\end{bmatrix} \quad (15)$$

TABLE I
COMPUTATIONAL COMPARISON

Step	Process	Direct MILS	CPS MILS
1)	Float solution	$\mathcal{O}((n_s K)^3) \times \mathfrak{I}_1$	$\mathcal{O}((n_s K)^3) \times \mathfrak{I}_1$
2a)	Integrate INS	$fKn_s \times \mathfrak{I}_2$	0
2b)	QR of A	$2M(N_s)^2 \times \mathfrak{I}_2$	$2(2m)(3)^2 \times \mathfrak{I}_2$
2c)	QRZ of $\bar{\mathbf{Q}}_A^\mathsf{T} B$	$2(2Km)m^2 \times \mathfrak{I}_2$	$2(2m)m^2 \times \mathfrak{I}_2$
2d)	Integer Search	$(*) \times \mathfrak{I}_2$	$(*) \times \mathfrak{I}_2$
3)	Integer Valid.	Km	Km

the cost function in (14) can be factored as [9]

$$\begin{aligned}\|\boldsymbol{r} + \mathbf{A}\delta\mathbf{X} + \mathbf{B}\delta\mathbf{N}\|^2 &= \left\| \begin{bmatrix} \mathbf{Q}_A^\mathsf{T} \\ \bar{\mathbf{Q}}_A^\mathsf{T} \end{bmatrix} \boldsymbol{r} + \begin{bmatrix} \mathbf{R}_A \\ \mathbf{0} \end{bmatrix} \delta\mathbf{X} + \begin{bmatrix} \mathbf{Q}_A^\mathsf{T}\mathbf{B} \\ \bar{\mathbf{Q}}_A^\mathsf{T}\mathbf{B} \end{bmatrix} \delta\mathbf{N} \right\|^2 \\ &= \left\| \mathbf{Q}_A^\mathsf{T}\boldsymbol{r} + \mathbf{R}_A\delta\mathbf{X} + \mathbf{Q}_A^\mathsf{T}\mathbf{B}\delta\mathbf{N} \right\|^2 + \left\| \bar{\mathbf{Q}}_A^\mathsf{T}\boldsymbol{r} + \bar{\mathbf{Q}}_A^\mathsf{T}\mathbf{B}\delta\mathbf{N} \right\|^2. \end{aligned} \tag{16}$$

Note that for any fixed $\delta\mathbf{N}$, the first term on the right-hand side of the above equation can be made equal to zero by an appropriate choice of $\delta\mathbf{X}$. Thus, solving the following ILS problem:

$$\min_{\delta\mathbf{N}\in\mathbb{Z}^m} \left\| \bar{\mathbf{Q}}_A^\mathsf{T}\boldsymbol{r} + \bar{\mathbf{Q}}_A^\mathsf{T}\mathbf{B}\delta\mathbf{N} \right\|^2 \tag{17}$$

yields the optimum of (14). Typically, the ILS solution has two steps: reduction and search [35]. Each iteration of the NMILS is that computationally expensive and multiple iterations may be required, this is caused by the need for relinearization in (13) this is caused by changes in $\hat{\mathbf{X}}$.

Increasing the length K of the CRT window enhances both accuracy and reliability at the expense of a higher computational load. Later in Section V-D, the computational load will be summarized in Table I and compared with the CPS algorithm that is developed herein.

The main contribution of this paper is an alternative approach to replace Step 2). The new approach requires a significantly lower computational load. The general method of proof will be to show first that the two approaches would be equivalent if the GPS measurement equations were linear and time invariant and then to develop bounds on the errors incurred due to the GPS measurement equation nonlinear effects and time variations. Because the bounds are small relative to the measurement noise, these errors are irrelevant for practical engineering purposes. The proposed method is inspired by the observation that in practice the optimal solution trajectory $\mathbf{X}^*$ (with integers resolved) is different only from the float solution $\hat{\mathbf{X}}$ in terms of a common 3-D position error to each state vector in the trajectory (see Fig. 2). The mathematical analysis in Section V verifies this observation.

IV. COMMON-POSITION-SHIFT ESTIMATION

This section presents the CPS method, which is a computationally efficient alternative to the original CRT method.

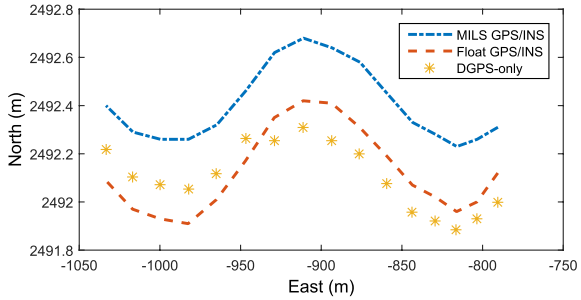

Fig. 2. Example comparison of horizontal positioning results. The blue dashed-dotted curve is from MILS GPS/INS [17] with centimeter accuracy. The red dashed curve shows the float solution from (12). The yellow asterisks show the DGPS differential pseudorange solution (i.e., no carrier phase).

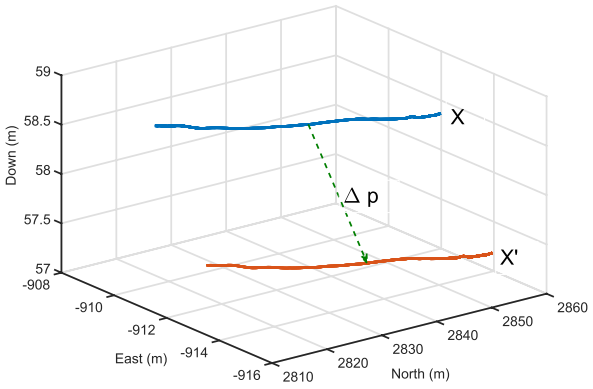

Fig. 3. Example 3-D position shift. The blue curve represents the original trajectory, the green dashed arrow represents the 3-D position shift vector, and the red curve represents the shifted trajectory.

The key point is to construct a smaller optimization problem to replace that in Step 2) of Section III. First, the notation for the CPS method is defined.

A. Notation of Common Position Shift

Given a trajectory $\mathbf{X} = [\boldsymbol{x}^\mathsf{T}(t_1), \ldots, \boldsymbol{x}^\mathsf{T}(t_K)]^\mathsf{T}$ and a CPS vector $\Delta\boldsymbol{p} \in \mathbb{R}^3$, define the CPS operator $\oplus$ as

$$\mathbf{X}' = \mathbf{X} \oplus \Delta\boldsymbol{p} \triangleq [\boldsymbol{x}^\mathsf{T}(t_1) \oplus \Delta\boldsymbol{p}, \ldots, \boldsymbol{x}^\mathsf{T}(t_K) \oplus \Delta\boldsymbol{p}]^\mathsf{T}$$

which denotes adding the constant vector $\Delta\boldsymbol{p}$ to the position portion $\boldsymbol{p}(t_k)$ of each state vector $\boldsymbol{x}(t_k)$ in $\mathbf{X}$. The resulting trajectory $\mathbf{X}'$ is referred to as the *shifted* trajectory with respect to the original $\mathbf{X}$ (see Fig. 3).

B. Outline of the CPS Method

This paper will show that the cost function $\|\boldsymbol{r}(\mathbf{X}, \mathbf{N})\|^2$ of (11) can be rewritten as a sum of cost functions

$$\|\boldsymbol{r}(\mathbf{X}, \mathbf{N})\|^2 = \|\boldsymbol{r_1}(\mathbf{X})\|^2 + \|\boldsymbol{r_2}(\mathbf{X})\|^2 + \|\boldsymbol{r_3}(\mathbf{X}, \mathbf{N})\|^2. \tag{18}$$

These cost functions have two important related properties. First, the term $\|\boldsymbol{r_1}(\mathbf{X})\|^2$ determines the shape, orientation, and general location of the trajectory, but is insensitive to a CPS $\Delta\boldsymbol{p}$ and to the integer vector $\mathbf{N}$ (see Proposition 2). Second, for any given $\mathbf{X}$, the terms $(\|\boldsymbol{r_2}(\mathbf{X})\|^2 + \|\boldsymbol{r_3}(\mathbf{X}, \mathbf{N})\|^2)$ are independent of $\mathbf{s}$ and can be minimized solely by the choice

of $(\Delta \boldsymbol{p}, \mathbf{N})$ (see Proposition 3). Therefore, if the linearization errors and the time variation of the GPS measurement model are ignored, Proposition 4 will show that the cost function can be rewritten as

$$\|\boldsymbol{r}(\mathbf{X}, \mathbf{N})\|^2 = \|\boldsymbol{r}_1(\check{\mathbf{X}})\|^2 + \|\boldsymbol{r}_2(\check{\mathbf{X}} \oplus \Delta \boldsymbol{p})\|^2 + \|\boldsymbol{r}_3(\check{\mathbf{X}} \oplus \Delta \boldsymbol{p}, \mathbf{N})\|^2$$

where $\mathbf{X} = \check{\mathbf{X}} \oplus \Delta \boldsymbol{p}$.

These facts allow the problem of interest to be solved by the following approach.

1) Find either the float solution $\check{\mathbf{X}}$ defined in (12) or the integer-free solution $\mathbf{X}^{\circledast}$ defined in (26), which are shown to be identical in Proposition 1.
2) Find $(\Delta \boldsymbol{p}^{\star}, \mathbf{N}^{\star})$ that is the optimal solution of

$$\min_{\Delta \boldsymbol{p} \in \mathbb{R}^3, \mathbf{N} \in \mathbb{Z}^m} \|\boldsymbol{r}_2(\check{\mathbf{X}} \oplus \Delta \boldsymbol{p})\|^2 + \|\boldsymbol{r}_3(\check{\mathbf{X}} \oplus \Delta \boldsymbol{p}, \mathbf{N})\|^2 \tag{19}$$

   where $\check{\mathbf{X}}$ is fixed when evaluating $\|\boldsymbol{r}_2\|^2 + \|\boldsymbol{r}_3\|^2$.
3) Check the validity of the integer estimates.

The trajectory-integer estimate from the CPS method is finalized as $(\check{\mathbf{X}} \oplus \Delta \boldsymbol{p}^{\star}, \mathbf{N}^{\star})$. The optimality of the solution $(\check{\mathbf{X}} \oplus \Delta \boldsymbol{p}^{\star}, \mathbf{N}^{\star})$ is discussed in Propositions 4 and 5 by comparing with $(\mathbf{X}^{*}, \mathbf{N}^{*})$ obtained from the original NMILS method revisited in Section III.

The CPS estimation in (19) is designed to replace the original full NMILS Step 2) in Section III. The optimization in (19) is also solved by the NMILS method outlined in Section III; however, the dimensions are significantly smaller and only a single (linearization) iteration is required.

C. Decomposition of GPS Cost Terms

This section defines the cost function decomposition for (18).

Define $\boldsymbol{\varphi}^i = [\varphi^i(t_1), \ldots, \varphi^i(t_K)]^{\intercal} \in \mathbb{R}^K$ to be the vector stacking the carrier phase measurements of the ith satellite. The last summation term in (9) can be rewritten as

$$\begin{aligned}
&\sum_k \sum_i \left\| h_k^i(\boldsymbol{x}(t_k)) + \lambda N^i - \varphi^i(t_k) \right\|_{\sigma_\varphi^2}^2 \\
&\quad = \sum_i \left[\sum_k \left\| h_k^i(\boldsymbol{x}(t_k)) + \lambda N^i - \varphi^i(t_k) \right\|_{\sigma_\varphi^2}^2 \right] \\
&\quad = \sum_i \|\boldsymbol{h}^i(\mathbf{X}) + \lambda \mathbf{1} N^i - \boldsymbol{\varphi}^i\|_{\sigma_\varphi^2 \mathbf{I}}^2
\end{aligned} \tag{20}$$

where $\boldsymbol{h}^i = [h_1^i(\boldsymbol{x}(t_1)), \ldots, h_K^i(\boldsymbol{x}(t_K))]^{\intercal} \in \mathbb{R}^K$, $\mathbf{1} = [1, \ldots, 1]^{\intercal} \in \mathbb{R}^K$, and $\mathbf{I}$ is the $K \times K$ identity matrix. In particular, $\mathbf{1}$ is rank 1 and can be QR decomposed as

$$[\mathcal{Q}_{\mathbf{1}}, \bar{\mathcal{Q}}_{\mathbf{1}}] \begin{bmatrix} \mathcal{R}_{\mathbf{1}} \\ \mathbf{0} \end{bmatrix} = \mathbf{1}$$

where[1] $[\mathcal{Q}_{\mathbf{1}}]_{1 \times K}$ and $[\bar{\mathcal{Q}}_{\mathbf{1}}]_{(K-1) \times K}$ contain orthonormal bases for the column space and the left null space of $\mathbf{1}$. Let $\mathcal{Q} = [\mathcal{Q}_{\mathbf{1}}, \bar{\mathcal{Q}}_{\mathbf{1}}]$, which is a unitary matrix. This QR decomposition can be computed offline for different K values.

[1]Note that $\mathcal{Q}_{\mathbf{1}}$ and $\mathbf{Q}_1$ are two different symbols. The former is the basis for the column space of $\mathbf{1}$. The latter is the covariance matrix of the first INS cost term in (9).

The ith term in (20) can be decomposed into two parts by projecting it on the column space and the left null space of $\mathbf{1}$

$$\begin{aligned}
&\|\boldsymbol{h}^i(\mathbf{X}) + \lambda \mathbf{1} N^i - \boldsymbol{\varphi}^i\|_{\sigma_\varphi^2 \mathbf{I}}^2 \\
&\quad = \|\mathcal{Q}^{\intercal}(\boldsymbol{h}^i(\mathbf{X}) + \lambda \mathbf{1} N^i - \boldsymbol{\varphi}^i)\|_{\mathcal{Q}^{\intercal} \sigma_\varphi^2 \mathcal{Q}}^2 \\
&\quad = \left\| \begin{bmatrix} \mathcal{Q}_{\mathbf{1}}^{\intercal} \\ \bar{\mathcal{Q}}_{\mathbf{1}}^{\intercal} \end{bmatrix} \left[\boldsymbol{h}^i(\mathbf{X}) + \lambda \mathcal{Q} \begin{bmatrix} \mathcal{R}_{\mathbf{1}} \\ \mathbf{0} \end{bmatrix} N^i - \boldsymbol{\varphi}^i \right] \right\|_{\sigma_\varphi^2 \mathbf{I}}^2 \\
&\quad = \left\| \begin{bmatrix} \mathcal{Q}_{\mathbf{1}}^{\intercal} \boldsymbol{h}^i(\mathbf{X}) + \lambda \mathcal{R}_{\mathbf{1}} N^i - \mathcal{Q}_{\mathbf{1}}^{\intercal} \boldsymbol{\varphi}^i \\ \bar{\mathcal{Q}}_{\mathbf{1}}^{\intercal}(\boldsymbol{h}^i(\mathbf{X}) - \boldsymbol{\varphi}^i) \end{bmatrix} \right\|_{\sigma_\varphi^2 \mathbf{I}}^2 \\
&\quad = \left\| \bar{\mathcal{Q}}_{\mathbf{1}}^{\intercal}(\boldsymbol{h}^i(\mathbf{X}) - \boldsymbol{\varphi}^i) \right\|_{\sigma_\varphi^2 \mathbf{I}^-}^2 \\
&\qquad + \left\| \mathcal{Q}_{\mathbf{1}}^{\intercal} \boldsymbol{h}^i(\mathbf{X}) + \lambda \mathcal{R}_{\mathbf{1}} N^i - \mathcal{Q}_{\mathbf{1}}^{\intercal} \boldsymbol{\varphi}^i \right\|_{\sigma_\varphi^2}^2
\end{aligned} \tag{21}$$

where $\mathbf{I}^- = \bar{\mathcal{Q}}_{\mathbf{1}}^{\intercal} \bar{\mathcal{Q}}_{\mathbf{1}}$ is the $(K-1) \times (K-1)$ identity matrix. Note that the first term in (21) is independent of the integer ambiguity N^i.

Applying the same QR factorization to the pseudorange summation term in (9) and reorganizing yield

$$\begin{aligned}
\|\boldsymbol{r}(\mathbf{X}, \mathbf{N})\|^2 = {} & \|\boldsymbol{s}(t_1) - \boldsymbol{s}_1\|_{\mathbf{P}_{s_1}}^2 \\
& + \sum_k \|\boldsymbol{\phi}(\boldsymbol{x}(t_k), \mathbf{U}_k) - \boldsymbol{x}(t_{k+1})\|_{\mathbf{Q}_k}^2 \\
& + \sum_i \left\| \bar{\mathcal{Q}}_{\mathbf{1}}^{\intercal}(\boldsymbol{h}^i(\mathbf{X}) - \boldsymbol{\rho}^i) \right\|_{\sigma_\rho^2 \mathbf{I}^-}^2 \\
& + \sum_i \left\| \bar{\mathcal{Q}}_{\mathbf{1}}^{\intercal}(\boldsymbol{h}^i(\mathbf{X}) - \boldsymbol{\varphi}^i) \right\|_{\sigma_\varphi^2 \mathbf{I}^-}^2 \\
& + \sum_i \left\| \mathcal{Q}_{\mathbf{1}}^{\intercal} \boldsymbol{h}^i(\mathbf{X}) - \mathcal{Q}_{\mathbf{1}}^{\intercal} \boldsymbol{\rho}^i \right\|_{\sigma_\rho^2}^2 \\
& + \sum_i \left\| \mathcal{Q}_{\mathbf{1}}^{\intercal} \boldsymbol{h}^i(\mathbf{X}) + \lambda \mathcal{R}_{\mathbf{1}} N^i - \mathcal{Q}_{\mathbf{1}}^{\intercal} \boldsymbol{\varphi}^i \right\|_{\sigma_\varphi^2}^2.
\end{aligned} \tag{22}$$

Based on the above expression, it will be convenient to define the following three cost functions. The first cost function

$$\begin{aligned}
\|\boldsymbol{r}_1(\mathbf{X})\|^2 \triangleq {} & \|\boldsymbol{s}(t_1) - \boldsymbol{s}_1\|_{\mathbf{P}_{s1}}^2 \\
& + \sum_k \|\boldsymbol{\phi}(\boldsymbol{x}(t_k), \mathbf{U}_k) - \boldsymbol{x}(t_{k+1})\|_{\mathbf{Q}_k}^2 \\
& + \sum_i \left\| \bar{\mathcal{Q}}_{\mathbf{1}}^{\intercal}(\boldsymbol{h}^i(\mathbf{X}) - \boldsymbol{\rho}^i) \right\|_{\sigma_\rho^2}^2 \\
& + \sum_i \left\| \bar{\mathcal{Q}}_{\mathbf{1}}^{\intercal}(\boldsymbol{h}^i(\mathbf{X}) - \boldsymbol{\varphi}^i) \right\|_{\sigma_\varphi^2 \mathbf{I}^-}^2
\end{aligned}$$

neglects the last two terms in (22). The second cost function is

$$\|\boldsymbol{r}_2(\mathbf{X})\|^2 \triangleq \sum_i \left\| \mathcal{Q}_{\mathbf{1}}^{\intercal} \boldsymbol{h}^i(\mathbf{X}) - \mathcal{Q}_{\mathbf{1}}^{\intercal} \boldsymbol{\rho}^i \right\|_{\sigma_\rho^2}^2. \tag{23}$$

The third cost function is

$$\|\boldsymbol{r}_3(\mathbf{X}, \mathbf{N})\|^2 \triangleq \sum_i \left\| \mathcal{Q}_{\mathbf{1}}^{\intercal} \boldsymbol{h}^i(\mathbf{X}) + \lambda \mathcal{R}_{\mathbf{1}} N^i - \mathcal{Q}_{\mathbf{1}}^{\intercal} \boldsymbol{\varphi}^i \right\|_{\sigma_\varphi^2}^2 \tag{24}$$

which will define the CPS and is analyzed in Section IV-B. With these definitions

$$\|\boldsymbol{r}(\mathbf{X}, \mathbf{N})\|^2 = \|\boldsymbol{r}_1(\mathbf{X})\|^2 + \|\boldsymbol{r}_2(\mathbf{X})\|^2 + \|\boldsymbol{r}_3(\mathbf{X}, \mathbf{N})\|^2. \tag{25}$$

To simplify expressions in the following discussion, let:

$$\|\boldsymbol{r}_a(\mathbf{X})\|^2 \triangleq \|\boldsymbol{r}_1(\mathbf{X})\|^2 + \|\boldsymbol{r}_2(\mathbf{X})\|^2$$
$$\|\boldsymbol{r}_b(\mathbf{X},\mathbf{N})\|^2 \triangleq \|\boldsymbol{r}_2(\mathbf{X})\|^2 + \|\boldsymbol{r}_3(\mathbf{X},\mathbf{N})\|^2.$$

D. Integer-Free Solution

Define the integer-free solution as

$$\mathbf{X}^{\circledast} = \arg\min_{\mathbf{X}\in\mathbb{R}^{n_s K}} \|\boldsymbol{r}_a(\mathbf{X})\|^2. \tag{26}$$

Proposition 1: If the variable $\mathbf{N}$ is treated as a real vector, then for $\check{\mathbf{X}}$ and $\check{\mathbf{N}}$, as defined in (12)

$$\|\boldsymbol{r}(\check{\mathbf{X}},\check{\mathbf{N}})\|^2 = \|\boldsymbol{r}_a(\mathbf{X}^{\circledast})\|^2$$

and $\mathbf{X}^{\circledast} = \check{\mathbf{X}}$, where $\boldsymbol{r}(\mathbf{X},\mathbf{N})$ is defined in (11). △

Proof 1: From (25)

$$\|\boldsymbol{r}(\mathbf{X},\mathbf{N})\|^2 = \|\boldsymbol{r}_1(\mathbf{X})\|^2 + \|\boldsymbol{r}_2(\mathbf{X})\|^2 + \sum_i \left\| \mathcal{Q}_{\mathbf{1}}^{\mathsf{T}}\boldsymbol{h}^i(\mathbf{X}) + \lambda\mathcal{R}_{\mathbf{1}}N^i - \mathcal{Q}_{\mathbf{1}}^{\mathsf{T}}\boldsymbol{\varphi}^i \right\|^2_{\sigma_\varphi^2}.$$

Each term in the summation is a scalar

$$||\mathcal{Q}_{\mathbf{1}}^{\mathsf{T}}\boldsymbol{h}^i(\mathbf{X}) + \lambda\mathcal{R}_{\mathbf{1}}N^i - \mathcal{Q}_{\mathbf{1}}^{\mathsf{T}}\boldsymbol{\varphi}^i||^2_{\sigma_\varphi^2}. \tag{27}$$

When N^i is treated as a real variable, then for any $\mathbf{X}$, the value

$$\check{N}^i = \frac{\mathcal{Q}_{\mathbf{1}}^{\mathsf{T}}(\boldsymbol{\varphi}^i - \boldsymbol{h}^i(\mathbf{X}))}{\lambda\mathcal{R}_{\mathbf{1}}} \tag{28}$$

makes the ith term zero. Therefore

$$\|\boldsymbol{r}(\mathbf{X},\check{\mathbf{N}})\| = \|\boldsymbol{r}_1(\mathbf{X})\|^2 + \|\boldsymbol{r}_2(\mathbf{X})\|^2.$$

□

Proposition 1 indicates that the integer-free solution is equivalent to the float solution of (12). This equivalence will be utilized in Section V.

V. Common-Position-Shift Method Analysis

This section presents the mathematical analysis of the proposed CPS method. With the aid of several propositions proved herein, the optimality of the CPS method is discussed in Propositions 4 and 5.

A. Useful Constants Related to GPS

In the analysis, certain GPS facts will be used [2], [3], [26]. They are summarized in this paragraph. The standard deviation of the differential pseudorange measurement is $\sigma_\rho = 0.5$–3 m. The standard deviation of the differential phase measurement is $\sigma_\varphi \approx 0.01\sigma_\rho$. The minimum distance from a receiver on the earth surface to a GPS satellite satisfies

$$h_k^i(\boldsymbol{p}_k) = \|\boldsymbol{p}(t_k) - \boldsymbol{p}^i(t_k)\| \geq \underline{D} \triangleq 20\,000 \text{ km}.$$

The orbital speed of the GPS satellite with respect to the ECEF origin satisfies $\|V^i\| \leq \bar{V} \triangleq 4.0$ km/s. When the DGPS base station is within a few tens of kilometers, DGPS accuracy is on the order of 1 m (i.e., 1σ) [3]. Herein, it is assumed that there are always base stations (e.g., from CORS [4]) available to the rover within 20 km. Therefore, for the float solution $\check{\mathbf{X}}$

$$\|\check{\boldsymbol{p}}(t_k) - \boldsymbol{p}(t_k)\| < \Delta_f = 3 \text{ m}.$$

B. Propositions for the CPS Method

Proposition 2 quantifies the sensitivity of $\|\boldsymbol{r}_1(\hat{\mathbf{X}})\|^2$ to a CPS.

Proposition 2: For any trajectory estimate, $\hat{\mathbf{X}} \in \mathbb{R}^{n_s K}$.

1) Neglecting the time variation and the high-order terms in the linearization of the GPS measurement model

$$\|\boldsymbol{r}_1(\hat{\mathbf{X}} \oplus \Delta\boldsymbol{p})\|^2 = \|\boldsymbol{r}_1(\hat{\mathbf{X}})\|^2. \tag{29}$$

2) Accounting for the time variation and the high-order terms in the linearization of the GPS measurement model, for any trajectory estimate $\hat{\mathbf{X}} \in \mathbb{R}^{n_s K}$ with $\|\Delta p\| < 10$ km, it is valid that

$$\bar{\mathcal{Q}}_{\mathbf{1}}^{\mathsf{T}}(\boldsymbol{h}^i(\hat{\mathbf{X}} \oplus \Delta\boldsymbol{p}) - \boldsymbol{\varphi}^i) = \bar{\mathcal{Q}}_{\mathbf{1}}^{\mathsf{T}}(\boldsymbol{h}^i(\hat{\mathbf{X}}) - \boldsymbol{\varphi}^i + \boldsymbol{\delta}_1) \tag{30}$$
$$\bar{\mathcal{Q}}_{\mathbf{1}}^{\mathsf{T}}(\boldsymbol{h}^i(\hat{\mathbf{X}} \oplus \Delta\boldsymbol{p}) - \boldsymbol{\rho}^i) = \bar{\mathcal{Q}}_{\mathbf{1}}^{\mathsf{T}}(\boldsymbol{h}^i(\hat{\mathbf{X}}) - \boldsymbol{\rho}^i + \boldsymbol{\delta}_1) \tag{31}$$

where $\boldsymbol{\delta}_1 \in \mathbb{R}^K$ is a vector of perturbations caused by the CPS. Furthermore, the magnitude of $\boldsymbol{\delta}_1$ is bounded by

$$\|\boldsymbol{\delta}_1\|_\infty \leq B_1(\|\Delta\boldsymbol{p}\|, \bar{v}) \tag{32}$$

where the real function $B_1 : \mathbb{R}_+^2 \mapsto \mathbb{R}_+$ is defined as

$$B_1(\|\Delta\boldsymbol{p}\|, \bar{v}) \triangleq K(C_1 + C_2\bar{v})\|\Delta\boldsymbol{p}\| + \|\Delta\boldsymbol{p}\|^2/2\underline{D} \tag{33}$$

and K is the CRT window length in seconds, $C_1 \triangleq (\bar{V}/\underline{D}) = 2.0 \times 10^{-4}$, $C_2 \triangleq (1/\underline{D}) = 5.0 \times 10^{-8}$ s/m, $\bar{v}$ is the upper bound of the rover speed over the window, and $\|\Delta\boldsymbol{p}\|$ is the magnitude of CPS. △

Proof 2: First, a CPS $\Delta\boldsymbol{p}$ will not cause any variation in the prior cost and the INS cost terms

$$\sum_k \|\boldsymbol{\phi}(\boldsymbol{x}(t_k \oplus \Delta\boldsymbol{p}), \mathbf{U}_k) - \boldsymbol{x}(t_{k+1} \oplus \Delta\boldsymbol{p})\|^2_{\mathbf{Q}_k} = \sum_k \|\boldsymbol{\phi}(\boldsymbol{x}(t_k), \mathbf{U}_k) - \boldsymbol{x}(t_{k+1})\|^2_{\mathbf{Q}_k}.$$

Therefore, the proof of (29) focuses on the GPS measurements. Equations (30) and (31) are first derived by considering the time variation and the high-order terms in the linearization of the GPS measurement model, and then by neglecting the perturbation $\boldsymbol{\delta}_1$ due to linearization errors, (29) is obtained.

With the assumption $\|\Delta\boldsymbol{p}\| < 10$ km, the numerical analysis in [1, Sec. 8.8.1.3] shows that

$$h_k^i(\boldsymbol{p}_k + \Delta\boldsymbol{p}) - h_k^i(\boldsymbol{p}_k) = H_k^i\Delta\boldsymbol{p} + \frac{\|\Delta\boldsymbol{p}\|^2}{2h_k^i(\boldsymbol{p}_k)} + \text{h.o.t.}$$

where $h_k^i(\boldsymbol{p}_k) = \|\boldsymbol{p}(t_k) - \boldsymbol{p}^i(t_k)\|$ and $H_k^i \in \mathbb{R}^{1\times 3}$ is the Jacobian matrix of h_k^i

$$H_k^i \triangleq H^i(t_k) = \frac{\partial h_k^i}{\partial \boldsymbol{p}(t_k)} = \left[\frac{\boldsymbol{p}(t_k) - \boldsymbol{p}^i(t_k)}{\|\boldsymbol{p}(t_k) - \boldsymbol{p}^i(t_k)\|}\right].$$

Given that $h_k^i(\boldsymbol{p}_k) \geq \underline{D}$ and $\epsilon_k^i \triangleq \|\Delta\boldsymbol{p}\|^2/(2h_k^i(\boldsymbol{p}_k))$, it follows that:

$$h_k^i(\boldsymbol{p}_k + \Delta\boldsymbol{p}) - h_k^i(\boldsymbol{p}_k) = H_k^i\Delta\boldsymbol{p} + \epsilon_k^i \tag{34}$$

with $|\epsilon_k^i| < \|\Delta\boldsymbol{p}\|^2/2\underline{D}$.

Consider $H^i(t) : \mathbb{R} \mapsto \mathbb{R}^3$ as a function of time

$$\bar{t} \triangleq (t_K + t_1)/2 \quad \text{and} \quad \bar{H}^i \triangleq H^i(\bar{t}) \tag{35}$$

then by Taylor series, it follows that:

$$H^i(t) = \bar{H}^i + \frac{dH^i(t)}{dt}(t - \bar{t}) + \text{h.o.t.} \tag{36}$$

By defining the variation

$$\check{H}^i_k \triangleq H^i_k - \bar{H}^i$$

and using (36), $\check{H}^i_k$ can be written as

$$\check{H}^i_k = \frac{dH^i(t_k)}{dt}(t_k - \bar{t}) + \text{h.o.t.}$$

The derivative $dH^i(t)/dt$ is

$$\frac{dH^i(t_k)}{dt} = \frac{\boldsymbol{v}(t) - \boldsymbol{v}^i(t)}{\|\boldsymbol{p}(t) - \boldsymbol{p}^i(t)\|} - \frac{(\boldsymbol{p}(t) - \boldsymbol{p}^i(t))(\boldsymbol{p}(t) - \boldsymbol{p}^i(t))^\intercal(\boldsymbol{v}(t) - \boldsymbol{v}^i(t))}{\|\boldsymbol{p}(t) - \boldsymbol{p}^i(t)\|^3} \tag{37}$$

and therefore, the variation of the Jacobian matrix is bounded by

$$\|\check{H}^i_k\| \leq \frac{2(\bar{v} + \bar{V})}{\underline{D}}|t_k - \bar{t}|$$

since $\|\boldsymbol{v}(t)\| \leq \bar{v}$ and $\|\boldsymbol{v}^i(t)\| \leq \bar{V}$. Furthermore, with Assumption 3, $(t_K - t_1) < K$ and then

$$\left\|\check{H}^i_k\right\| \leq \frac{\bar{V} + \bar{v}}{\underline{D}}(t_K - t_1) = K(C_1 + C_2\bar{v}). \tag{38}$$

We are now in a position to consider the effect of a shift $\Delta\boldsymbol{p}$ on the value of $\bar{\mathcal{Q}}_{\mathbf{1}}^\intercal \boldsymbol{h}^i(\hat{\mathbf{X}} \oplus \Delta\boldsymbol{p})$

$$\begin{aligned}
\bar{\mathcal{Q}}_{\mathbf{1}}^\intercal \boldsymbol{h}^i(\hat{\mathbf{X}} \oplus \Delta\boldsymbol{p}) &= \bar{\mathcal{Q}}_{\mathbf{1}}^\intercal \begin{bmatrix} h^i_1(\hat{\boldsymbol{p}}_1 + \Delta\boldsymbol{p}) \\ \vdots \\ h^i_K(\hat{\boldsymbol{p}}_K + \Delta\boldsymbol{p}) \end{bmatrix} \\
&= \bar{\mathcal{Q}}_{\mathbf{1}}^\intercal \begin{bmatrix} h^i_1(\hat{\boldsymbol{p}}_1) + H^i_1\Delta\boldsymbol{p} + \epsilon^i_1 \\ \vdots \\ h^i_K(\hat{\boldsymbol{p}}_K) + H^i_K\Delta\boldsymbol{p} + \epsilon^i_K \end{bmatrix} \\
&= \bar{\mathcal{Q}}_{\mathbf{1}}^\intercal \begin{bmatrix} h^i_1(\hat{\boldsymbol{p}}_1) \\ \vdots \\ h^i_K(\hat{\boldsymbol{p}}_K) \end{bmatrix} + \bar{\mathcal{Q}}_{\mathbf{1}}^\intercal \begin{bmatrix} H^i_1 \\ \vdots \\ H^i_K \end{bmatrix} \Delta\boldsymbol{p} + \bar{\mathcal{Q}}_{\mathbf{1}}^\intercal \boldsymbol{\epsilon}^i
\end{aligned}$$

where for ϵ^i_k in (34)

$$\boldsymbol{\epsilon}^i \triangleq \left[\epsilon^i_1, \ldots, \epsilon^i_K\right]^\intercal \in \mathbb{R}^K. \tag{39}$$

With the notation of $\bar{H}^i$ and $\check{H}^i_k$, it follows that:

$$\begin{aligned}
&\bar{\mathcal{Q}}_{\mathbf{1}}^\intercal \boldsymbol{h}^i(\hat{\mathbf{X}} \oplus \Delta\boldsymbol{p}) \\
&\quad = \bar{\mathcal{Q}}_{\mathbf{1}}^\intercal \boldsymbol{h}^i(\hat{\mathbf{X}}) + \bar{\mathcal{Q}}_{\mathbf{1}}^\intercal \begin{bmatrix} \check{H}^i_1 \\ \vdots \\ \check{H}^i_K \end{bmatrix} \Delta\boldsymbol{p} + \bar{\mathcal{Q}}_{\mathbf{1}}^\intercal \begin{bmatrix} \bar{H}^i\Delta\boldsymbol{p} \\ \vdots \\ \bar{H}^i\Delta\boldsymbol{p} \end{bmatrix} + \bar{\mathcal{Q}}_{\mathbf{1}}^\intercal \boldsymbol{\epsilon}^i \\
&\quad = \bar{\mathcal{Q}}_{\mathbf{1}}^\intercal \left(\boldsymbol{h}^i(\hat{\mathbf{X}}) + \begin{bmatrix} \check{H}^i_1 \\ \vdots \\ \check{H}^i_K \end{bmatrix} \Delta\boldsymbol{p} + \boldsymbol{\epsilon}^i \right) + \mathbf{0}
\end{aligned}$$

where the $\mathbf{0}$ term follows from the fact that the columns of $\bar{\mathcal{Q}}_{\mathbf{1}}$ span the left null space of $\mathbf{1}$. Thus, it follows that:

$$\bar{\mathcal{Q}}_{\mathbf{1}}^\intercal \boldsymbol{h}^i(\hat{\mathbf{X}} \oplus \Delta\boldsymbol{p}) = \bar{\mathcal{Q}}_{\mathbf{1}}^\intercal [\boldsymbol{h}^i(\hat{\mathbf{X}}) + \boldsymbol{\delta}_1] \tag{40}$$

with the perturbation

$$\boldsymbol{\delta}_1 \triangleq \left[\check{H}^i_1\Delta\boldsymbol{p} + \epsilon^i_1, \ldots, \check{H}^i_K\Delta\boldsymbol{p} + \epsilon^i_K\right]^\intercal. \tag{41}$$

Then, from (38) it follows that:

$$\begin{aligned}
\|\boldsymbol{\delta}_1\|_\infty &= \max\left\{|\check{H}^i_k\Delta\boldsymbol{p} + \epsilon^i_1|\right\} \\
&\leq K(C_1 + C_2\bar{v})\|\Delta\boldsymbol{p}\| + \|\Delta\boldsymbol{p}\|^2/2\underline{D}
\end{aligned}$$

where $C_1 = 2.0 \times 10^{-4}$ and $C_2 = 5.0 \times 10^{-8}$ s/m.

With (40), (30) and (31) can be derived, and then by neglecting the perturbation $\boldsymbol{\delta}_1$, (29) is valid.

Remark 3: The intuition behind Proposition 2 is that due to the small variation in $\boldsymbol{h}^i(\boldsymbol{p}(t))$, for small time windows and small perturbations $\Delta\boldsymbol{p}$, their effect is removed by the linear transformation $\bar{\mathcal{Q}}^\intercal$. For typical values (i.e., $K \leq 10$, $\|\Delta\boldsymbol{p}\| \leq 1.5$ m, and $\bar{v} \leq 50$ m/s) the upper bound on the perturbation $\|\check{H}^i_k\Delta\boldsymbol{p}\|$ caused by the CPS is 0.0031 m, which is a factor of ten smaller than the centimeter noise level of the carrier phase measurement. Because the perturbation is small relative to the carrier phase measurement noise and multipath, they can be neglected. △

Proposition 3 considers the cost functions $\|\boldsymbol{r}_2(\mathbf{X})\|^2$ and $\|\boldsymbol{r}_3(\mathbf{X}, \mathbf{N})\|^2$ defined in (23) and (24).

Proposition 3: Consider any two trajectory integer estimates $(\hat{\mathbf{X}}_1, \hat{\mathbf{N}}_1)$ and $(\hat{\mathbf{X}}_2, \hat{\mathbf{N}}_2)$.

1) Neglecting the time variation and the high-order terms in the linearization of the GPS measurement model, there exists a correction $(\Delta\boldsymbol{p}, \delta\mathbf{N}) \in \mathbb{R}^3 \times \mathbb{Z}^m$ such that

$$\begin{aligned}
&\|\boldsymbol{r}_{\mathbf{2}}(\hat{\mathbf{X}}_1 \oplus \Delta\boldsymbol{p})\|^2 + \|\boldsymbol{r}_{\mathbf{3}}(\hat{\mathbf{X}}_1 \oplus \Delta\boldsymbol{p}, \hat{\mathbf{N}}_1 + \delta\mathbf{N})\|^2 \\
&\qquad = \|\boldsymbol{r}_{\mathbf{2}}(\hat{\mathbf{X}}_2)\|^2 + \|\boldsymbol{r}_{\mathbf{3}}(\hat{\mathbf{X}}_2, \hat{\mathbf{N}}_2)\|^2.
\end{aligned} \tag{42}$$

2) Define the position errors between trajectories $\hat{\mathbf{X}}_1$ and $\hat{\mathbf{X}}_2$ as $\delta\mathbf{p}_k \triangleq \boldsymbol{p}^2_k - \boldsymbol{p}^1_k, k = 1, \ldots, K$. Accounting for the time variation and the high-order terms in the linearization of the GPS measurement model, if $\|\delta\boldsymbol{p}_k\| < 10$ km, there exists a correction $(\Delta\boldsymbol{p}, \delta\mathbf{N}) \in \mathbb{R}^3 \times \mathbb{Z}^m$ such that

$$\begin{aligned}
&\mathcal{Q}_{\mathbf{1}}^\intercal \boldsymbol{h}^i(\hat{\mathbf{X}}_1 \oplus \Delta\boldsymbol{p}) + \lambda\mathcal{R}_{\mathbf{1}}\left(\hat{N}^i_1 + \delta N^i\right) - \mathcal{Q}_{\mathbf{1}}^\intercal \boldsymbol{\varphi}^i \\
&\qquad = \mathcal{Q}_{\mathbf{1}}^\intercal \boldsymbol{h}^i(\hat{\mathbf{X}}_2) + \lambda\mathcal{R}_{\mathbf{1}}\hat{N}^i_2 - \mathcal{Q}_{\mathbf{1}}^\intercal \boldsymbol{\varphi}^i + \mathcal{Q}_{\mathbf{1}}^\intercal \boldsymbol{\delta}_2
\end{aligned} \tag{43}$$

$$\begin{aligned}
&\mathcal{Q}_{\mathbf{1}}^\intercal \boldsymbol{h}^i(\hat{\mathbf{X}}_1 \oplus \Delta\boldsymbol{p}) - \mathcal{Q}_{\mathbf{1}}^\intercal \boldsymbol{\rho}^i \\
&\qquad = \mathcal{Q}_{\mathbf{1}}^\intercal \boldsymbol{h}^i(\hat{\mathbf{X}}_2) - \mathcal{Q}_{\mathbf{1}}^\intercal \boldsymbol{\rho}^i + \mathcal{Q}_{\mathbf{1}}^\intercal \boldsymbol{\delta}_2
\end{aligned} \tag{44}$$

where the magnitude of $\boldsymbol{\delta}_2$ is bounded by

$$\|\boldsymbol{\delta}_2\|_\infty \leq B_1(\|\Delta\boldsymbol{p}\|, \bar{v}) \tag{45}$$

where B_1 and $\bar{v}$ are defined in (33). △

Proof 3: The details of this proof are in Appendix II.

Remark 4: Proposition 3 shows when K and $\|\Delta\boldsymbol{p}\|$ are bounded (e.g., $K \leq 10$ and $\|\Delta\boldsymbol{p}\| \leq 3$ m), we can minimize $\|\boldsymbol{r}_2(\mathbf{X})\|^2 + \|\boldsymbol{r}_3(\mathbf{X}, \mathbf{N})\|^2$ to within a small error, just through a CPS $\Delta\boldsymbol{p}$ and adjusting the integer estimates by $\delta\mathbf{N}$. Furthermore, the magnitude of the error $\boldsymbol{\delta}_2$ is small relative to

the noise level of carrier phase measurements. For example, for $K \leq 10$, $\Delta_p \leq 1.5$ m, and $\bar{v} \leq 50$ m/s, it follows that $\|\boldsymbol{\delta}_2\|_\infty \leq 0.0031$ m. △

C. Optimality of the CPS Method

The major propositions about the optimality of the CPS method are presented as follows.

Proposition 4: If $\boldsymbol{\delta}_1 = \mathbf{0}$ and $\boldsymbol{\delta}_2 = \mathbf{0}$, then the following identity is valid:

$$\|\boldsymbol{r}(\check{\mathbf{X}} \oplus \Delta\boldsymbol{p}^\star, \mathbf{N}^\star)\|^2 = \|\boldsymbol{r}(\mathbf{X}^*, \mathbf{N}^*)\|^2 \tag{46}$$

where $\check{\mathbf{X}}$ is the float solution from (12), $(\Delta\boldsymbol{p}^\star, \mathbf{N}^\star)$ is the CPS solution from (19), and $(\mathbf{X}^*, \mathbf{N}^*)$ is the full NMILS estimate from (11). △

Proof 4: See Appendix III.

Remark 5: This paper and proof introduce different trajectories $\check{\mathbf{X}}$, $\mathbf{X}^*$, and $\mathbf{X}^{\circledast}$ and trajectory sets $\mathbf{X}_1^*$, $\mathbf{X}_2^*$ and $\mathbf{X}_\star$. The proof shows that certain components of the cost function have the same value when evaluated for different trajectories or trajectory sets. Taking advantage of this allows definition of the CPS algorithm described in (19) that vastly reduces the computational load, as summarized in Table I. △

Proposition 4 considers the case where the linearization errors do not exist. Proposition 5 analyzes the effect of the linearization errors.

Proposition 5: Accounting for the time variation and the high-order terms in the linearization of the GPS measurement model, the following inequality is valid:

$$\boldsymbol{E}\{\|\boldsymbol{r}(\check{\mathbf{X}} \oplus \Delta\boldsymbol{p}^\star, \mathbf{N}^\star)\|^2\} \leq (1 + C_3)\boldsymbol{E}\{\|\boldsymbol{r}(\mathbf{X}^*, \mathbf{N}^*)\|^2\}$$

where $\check{\mathbf{X}}$ is the float solution from (12), $(\Delta\boldsymbol{p}^\star, \mathbf{N}^\star)$ is the CPS solution from (19) with $\|\Delta\boldsymbol{p}^\star\| \leq \Delta_f$, and

$$C_3 = \frac{Km\left(4\sigma_\rho^{-2} + 3\sigma_\varphi^{-2}\right)[B_1(\Delta_f, \bar{v})]^2}{(2K-1)m - 3}$$

and $(\mathbf{X}^*, \mathbf{N}^*)$ is the full NMILS estimate from (11) and $\boldsymbol{E}\{\cdot\}$ is the expectation operator. △

Proof 5: See Appendix IV.

Remark 6: When $K = 10$, $\Delta_f = 1.5$, $m = 7$, $\sigma_\rho = 1.0$ m and $\sigma_\varphi = 0.020$ m, and $C_3 = 0.04$. The error between the expected final costs of two optimizations is bounded within 4% of the expected optimum from the full NMILS approach. For the full NMILS solution, the residuals are at the centimeter level; therefore, the worst case perturbations would be 0.4 mm. Thus, Propositions 4 and 5 show that the CPS is a valid and accurate approximation to the original full NMILS approach. △

The implementation results presented in Section VI demonstrate that the differences between two approaches match the expected performance.

D. Computation Analysis of the CPS Method

Table I compares the computational cost of the direct MILS (see Section III) and CPS MILS (see Section IV-A).

TABLE II
EXAMPLE COMPARISON OF COMPUTATIONAL LOAD: $f = 200$, $K = 10$, $n_s = 16$, $N_s = 160$, $M = 297$, AND $m = 7$

Step	Direct MILS	CPS MILS
2a)	$3.20 \times 10^4 \times \mathfrak{I}_2$	0
2b)	$1.52 \times 10^7 \times \mathfrak{I}_2$	$2.52 \times 10^2 \times \mathfrak{I}_2$
2c)	$1.37 \times 10^4 \times \mathfrak{I}_2$	$1.37 \times 10^3 \times \mathfrak{I}_2$

In Table I, $\mathfrak{I}_1$ represents the number of (linearized) nonlinear least squares iterations required to find in the float solution of Step 1). Similarly, $\mathfrak{I}_2$ represents the number of linearized iterations required for integer ambiguity resolution in the ILS problem of Step 2). The IMU sampling rate (e.g., 200 Hz) is f.

Compared with solving the full NMILS in (11) directly, the computational cost in (19) is significantly reduced due to the much smaller dimension of the real unknown variable $\Delta\boldsymbol{p} \in \mathbb{R}^3$ versus $\mathbf{X} \in \mathbb{R}^{n_s K}$. In particular, this dimension reduction facilitates the QR decomposition in (15) [see Row (2b) in Table I]. The dimensions of the corresponding A matrices in the full MILS and CPS MILS are $M \times N_s$ versus $2m \times 3$, where $M \triangleq n_s K + 2mK - 3$ is the dimension of the residual vector, $N_s \triangleq n_s K$ is the total state dimension of $\mathbf{X}$, and $2m$ is the total number of GPS measurements at a single epoch (code and carrier phase). Furthermore, while each NMILS iteration of the direct approach requires the expensive INS reintegration, the CPS NMILS of (19) does not [see Row (2a) in Table I]. In the ILS, the reduction step is cast as a QRZ decomposition, which is actually a QR factorization with column pivoting (or column reordering) [35]. In CPS MILS, the computation cost on QRZ decomposition is lower due to the smaller dimension of $\bar{\mathbf{Q}}_A^\intercal B$ [see Row (2c) in Table I]. On the other hand, the computation of the integer search represented with $(*)$ in Row (2d) of Table I will not vary significantly, since the dimension of $\delta\mathbf{N}$ is the same in both approaches. The computation of the float solution and the integer validation is the same in both the direct MILS and CPS MILS methods.

To give a better sense of the computation improvement achieved by the CPS approach, Table II shows an numerical example of computation costs in Row (2a–c) of Table I. In this example, the IMU frequency is 200 Hz, the CRT window length is $K = 10$ epochs, the dimension of navigation state is $n_s = 16$, the average GNSS satellite availability is $m = 7$, $N_s = 160$, and $M = 297$. Table II indicates in each step that the CPS approach saves at least 90% of computation. In particular, the computation cost of the QR decomposition in Step 2*b*) is significantly reduced by an order of 10^5.

Note that neither approach being compared involved any type of algorithm that would reduce computations by taking into account the significant level of sparsity in the matrix A. Sparse matrix implementations are an area of future research that could further significantly reduce the computational load.

VI. EXPERIMENTS

This section discusses the experimental implementations of the proposed CPS method. The results demonstrate that

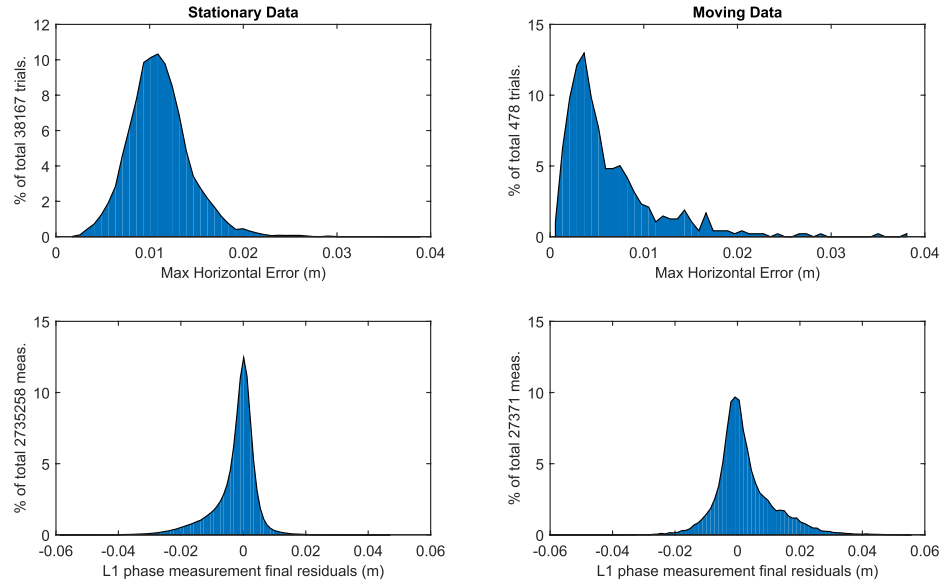

Fig. 4. Maximum norm of horizontal positioning error and posterior L1 phase measurements residuals within each $K = 10$-s CRT window for the CPS method.

the CPS state estimates are close to those of the original approach.

A. Solution Validation

In addition to the integer validation techniques, a threshold Δ_f for the CPS is used as a sanity check. This threshold can be picked by the designer based on the expected positioning accuracy of the float solution. After the CPS estimation in (19), if $\|\Delta \boldsymbol{p}^\star\| < \Delta_f$ and $\mathbf{N}^\star$ can be validated with standard integer validation techniques [31], then the estimate of $(\mathbf{X}, \mathbf{N})$ that resulted from this CPS approach is finalized as $(\check{\mathbf{X}} \oplus \Delta \boldsymbol{p}^\star, \mathbf{N}^\star)$.

Various alternatives are possible if the CPS solution is invalidated. The residuals could be analyzed in an attempt to detect and remove satellites with noisy or invalid measurements to improve performance within the current epoch. The original full NMILS in (11) could be executed to attempt to get $(\mathbf{X}^*, \mathbf{N}^*)$. Alternatively, the float solution $\check{\mathbf{X}}$ could be used to update the real-time state estimates, while at future epochs, the CRT window could be augmented with additional data for the next trial of integer resolution. For example, the designer can choose to slide the current window to the next epoch(s) or extend the length of the current window to accumulate more data. Or the scheme could just skip the current window and wait for a new window with larger m, which should yield a higher success rate. In the following experiments, $\Delta_f = 3$ m.

B. Experimental Description

For performance evaluation, the proposed approach is implemented in C++ and applied to RTK GPS/INS data sets collected from an automotive vehicle. The on-vehicle GPS/INS suite consists of a NovAtel OEMV3 receiver that outputs GPS pseudorange and carrier phase measurements at 1 Hz, and a 200-Hz NV-IMU1000 IMU from NAV Technology Company Ltd that outputs the specific forces and angular rate measurements along the three orthogonal axes. The DGPS information, including the raw dual-frequency GPS measurements (Message 1004 in RTCM3.1) and the base position (Message 1006 in RTCM3.1), is broadcast by the UC Riverside (UCR) Ntrip Caster (ntrip.engr.ucr.edu:2101) publicly over the Internet at 1 and 0.1 Hz, respectively [36], [37].

Two data sets logged on the vehicle are processed by the CPS approach:

1) a stationary 12-h (43 200-s) data set collected on UCR campus on March 29, 2014;
2) a moving 640-s data set collected while driving near the UCR Center for Environmental Research and Technology (CE-CERT) on January 23, 2014.

Since the purpose of the IMU is to cause the residuals to be insensitive to vehicle motion, the performance (i.e., position error and residual analysis) on the two data sets should be similar. The accuracy of the stationary data is more easily verified.

The algorithms were executed on a desktop computer with Intel Core2 Q9400 four-core CPU at 2.66 GHz, 8-GB DDR3 1333-MHz memory, and 240-GB SSD disk drive. The program runs in Ubuntu 12.04 64-bit OS within a VMware virtual machine for Windows 7. The total memory used by the virtual machine is up to 4 GB. Under this implementation environment and picking the CRT window length to be $K = 10$ s, the average computing time for one CPS iteration is approximately 0.25 ms versus 150 ms for the original full MILS method, indicating significant (600×) computational performance improvement. The code is capable of real-time or postprocessed modes of operation. The results presented here are from postprocessing, still running in real time, using stored data.

For the stationary data, the 3-D ground-truth position is known, so positioning errors are presented to show the CPS performance. For the moving data sets, the ground truth is unavailable; therefore, the trajectory and integer estimates

from the CPS and the original full MILS method [17] are compared to show that the CPS is an efficient alternative to the full MILS method, while achieving the same level of accuracy. For both implementations, dual-frequency carrier phase measurements are utilized to form wide-lane phase measurements [1]. For both stationary and moving data, histograms of the L1 carrier phase measurements residuals are used as a second method to illustrate CRT accuracy. A 10° elevation mask is applied to GPS satellites. Integers were resolved only when the CRT windows contained at least five satellites. In the evaluation of the CPS approach, the initial condition and the prior term in the cost function of (9) include only $\boldsymbol{s}$ defined in (3). There is no prior for the position or integer. Therefore, the integer solutions for each CRT window are independent. After estimation at each time step, a residual check is used to validate the integer estimates. If the magnitude of a carrier phase measurement residuals with fixed integer estimate is larger than 0.06 m, the integer estimate is rejected. Other integer validation techniques, e.g., ratio test, can be applied [31], [38]. Only the validated results are recorded.

C. Stationary Data

For the stationary data, the antenna position $\boldsymbol{p}_0$ is surveyed with accuracy at the millimeter level. The algorithm itself has no knowledge of this ground-truth position.

For each 10-s CRT windows, the algorithm estimates $\mathbf{X} = [\boldsymbol{x}(t_1)^\mathsf{T}, \boldsymbol{x}(t_2)^\mathsf{T}, \ldots, \boldsymbol{x}(t_{10})^\mathsf{T}]^\mathsf{T}$. For the 43 200-s stationary data, 569 trials failed with $m < 5$, 38 167 trials are validated (i.e., $m \geq 5$ and the residual check is passed). The positioning results are presented through comparison with the ground truth (i.e., $\boldsymbol{p}(t_k) - \boldsymbol{p}_0$). To evaluate the positioning performance, the *maximum* norm of the horizontal position error over each CRT window was logged and is shown as a histogram in Fig. 4 (top-left). Accuracies below 0.02 m are typical, which matches the expected performance of RTK GPS positioning. Fig. 4 (bottom-left) shows that the vast majority of the L1 phase residuals lie in $[-0.02, 0.02]$ m.

D. Moving Data

The route and satellite availability while logging this data set are shown in Fig. 5. The average vehicle speed is 35 km/h.

Since the ground truth is not available for this data set, the implementation results of the CPS method are compared with those of the original full MILS method [17]. The implementation results show that all the validated integers from CPS are identical to those from the full MILS method. Furthermore, Fig. 4 (top-right) shows that the maximum norm, during each CRT window, of the horizontal position error between CPS and full MILS are bounded by 0.04 m and typically less than 0.02 m. This demonstrates that the CPS method is a good approximation of the full MILS method in terms of integer ambiguity resolution and positioning. Fig. 4 (bottom-right) shows that most of the L1 phase measurement residuals lie in $[-0.02, 0.02]$ m.

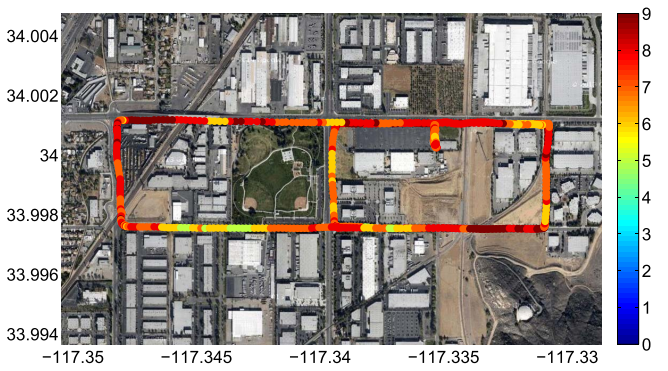

Fig. 5. Route and the satellite availability of the 640-s moving data experiment. The x- and y-axis are the longitude and latitude in degrees, respectively. The colors along the route indicate the number of satellites visible to the receiver at that location and time.

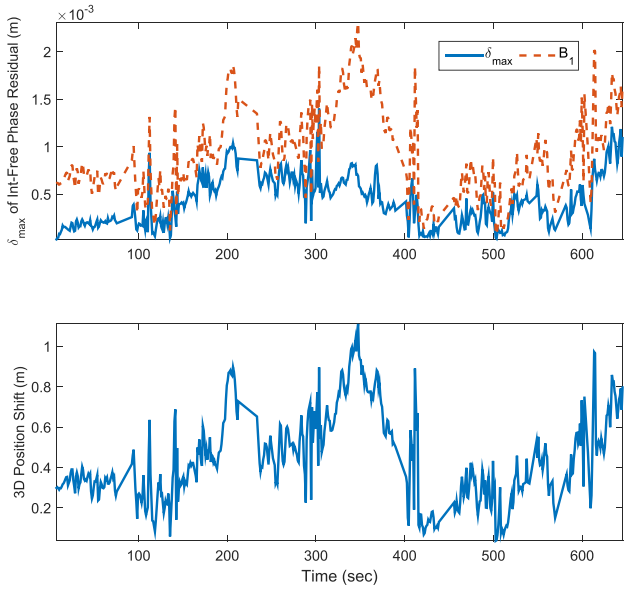

Fig. 6. Magnitude of the 3-D position shift estimated by CPS and the variations of $\|\boldsymbol{r}_4\|^2$ caused by the CPS.

The purpose of Fig. 6 is to validate Proposition 2. For the ith satellite in each time window, define

$$\Delta \boldsymbol{r}^i \triangleq \bar{\mathcal{Q}}_1^\mathsf{T}(\boldsymbol{h}^i(\check{\mathbf{X}} \oplus \Delta \boldsymbol{p}^\star) - \boldsymbol{\varphi}^i) - \bar{\mathcal{Q}}_1^\mathsf{T}(\boldsymbol{h}^i(\check{\mathbf{X}}) - \boldsymbol{\varphi}^i)$$

which is the variation of the integer-free phase measurement residuals (see Proposition 2) caused by the estimated CPS $\Delta \boldsymbol{p}^\star$. Furthermore, $\Delta \boldsymbol{r}^i$ can be rewritten as

$$\Delta \boldsymbol{r}^i = \bar{\mathcal{Q}}_1^\mathsf{T}(\boldsymbol{h}^i(\check{\mathbf{X}} \oplus \Delta \boldsymbol{p}^\star) - \boldsymbol{h}^i(\check{\mathbf{X}})).$$

For the moving data, the maximum magnitude of $\Delta \boldsymbol{r}^i$ over each CRT window, i.e., $\boldsymbol{\delta}_{\max} = \max_i\{\|\Delta \boldsymbol{r}^i\|_\infty\}$, is recorded along with the magnitude of CPS $\|\Delta \boldsymbol{p}^\star\|$ for each CRT window.

Proposition 2 implies that a CPS will cause only small variations, $\Delta \boldsymbol{r}^i$, that are upper bounded by $B_1(\|\Delta \boldsymbol{p}^\star\|, \bar{v})$. Fig. 6 validates this claim by plotting $\boldsymbol{\delta}_{\max}$, $\|\Delta \boldsymbol{p}^\star\|$, and the bound B_1 calculated in (33). Fig. 6 also shows that in this data set, all the CPS estimates have norm less than 1.2 m, as expected.

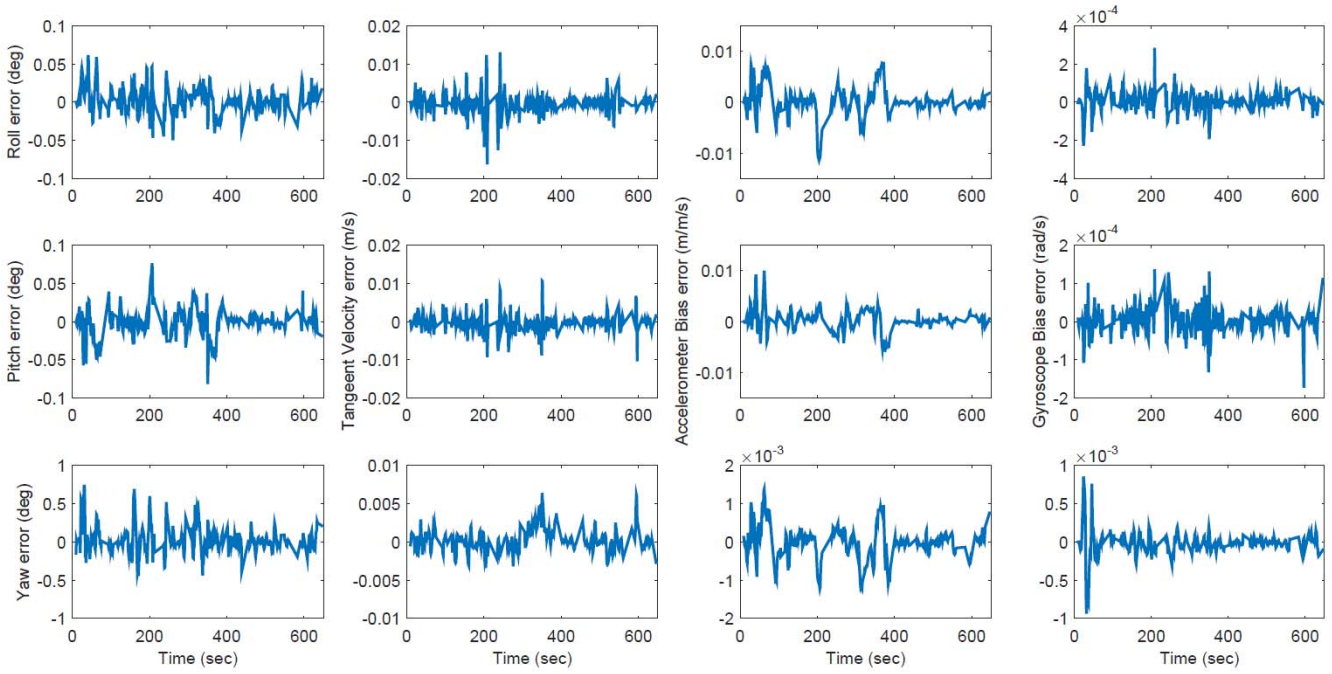

Fig. 7. Maximum attitude, velocity, and bias estimation errors between the CPS and full MILS results of the moving data.

Fig. 7 shows the maximum differences between the CPS estimates and the full MILS estimates of attitude, velocity, and bias. Fig. 7 shows that the roll and pitch estimate errors are smaller than 0.1°, and for yaw angle, most of the errors are smaller than 0.5°. The velocity estimate errors between two methods are smaller than 0.02 m/s.

VII. Conclusion

This paper proposes a novel integer ambiguity resolution approach over a time window of GPS/IMU data. The purpose of processing a window of data is to enhance the reliability of obtaining high-accuracy position estimation, using carrier phase measurements, even in challenging environments. Enhanced reliability will require further research into outlier detection methods that are beyond the scope of this paper.

The CPS method focuses on the reduction of computational cost. Theoretically, the achievable computational savings should be on the order of 10^4, while 600 has been demonstrated. Future research could further reduce the computational load by taking advantage of the potential sparsity of the linearized matrix denoted by A. The analysis shows that the estimation accuracy of the original and CPS algorithms would be identical if the GPS measurements were linear and time invariant and presents bounds on the errors incurred due to the measurement nonlinearity and time dependence.

The theoretical approach is also interesting in that it shows that the cost function can be decomposed into one part that determines the shape and vicinity of the trajectory, but is insensitive to the carrier phase integers and a position shift vector, and a second part that is sensitive to the carrier phase integer and can be solved to determine the required position shift so that the location of the trajectory is accurately known.

Theoretical analysis is presented for the CPS method. The implementation results show that the proposed CPS method obtains integer estimates identical to those from the original full MILS method and obtains centimeter positioning accuracy and that other state estimation errors are small.

Appendix I
INS Review

For any initial state $\boldsymbol{x}(\tau_k)$, the solution to (1) for $t \in [\tau_k, \tau_{k+1}]$ is

$$\boldsymbol{x}(t) = \boldsymbol{x}(\tau_k) + \int_{\tau_k}^{t} \boldsymbol{f}(\boldsymbol{x}(\tau), \boldsymbol{u}(\tau))d\tau. \tag{47}$$

While nature solves (47) in continuous time, the INS has only IMU and aiding measurements at discrete-time instants; therefore, the INS numerically solves

$$\begin{aligned}\hat{\boldsymbol{x}}(\tau_{k+1}) &= \boldsymbol{\phi}(\hat{\boldsymbol{x}}(\tau_k), \tilde{\boldsymbol{u}}(\tau_k)) \\ &= \hat{\boldsymbol{x}}(\tau_k) + \int_{\tau_k}^{\tau_{k+1}} \boldsymbol{f}(\hat{\boldsymbol{x}}(\tau), \tilde{\boldsymbol{u}}(\tau))d\tau \end{aligned} \tag{48}$$

where $\boldsymbol{\phi}$ is defined as the integration operator. The result of the numeric integration of (48) is the INS state estimate of $\hat{\boldsymbol{x}}(\tau_{k+1})$ for the given $\hat{\boldsymbol{x}}(\tau_k)$ and $\hat{\boldsymbol{u}}(\tau_k)$. The numeric integration repeats to propagate the state measurements between the times of aiding measurements. The aiding measurement times can be unequally spaced in time without causing any complications.

Let $\tilde{\mathbf{U}}_j = \{\tilde{\boldsymbol{u}}(\tau_k),\ \tau_k \in [t_j, t_{j+1}]\}$, then (48) can be called recursively to compute $\hat{\boldsymbol{x}}(t_{j+1})$ from $\hat{\boldsymbol{x}}(t_j)$ and $\tilde{\mathbf{U}}_j$; denote this by $\hat{\boldsymbol{x}}(t_{j+1}) = \boldsymbol{\phi}(\hat{\boldsymbol{x}}(t_j), \tilde{\mathbf{U}}_j)$. At the same time, nature is integrating (47) which it denoted as $\boldsymbol{x}(t_{j+1}) = \boldsymbol{\phi}(\boldsymbol{x}(t_j), \mathbf{U}_j)$. The linearized error growth model is

$$\delta\hat{\boldsymbol{x}}(t_{j+1}) = \boldsymbol{\Phi}_j \delta\hat{\boldsymbol{x}}(t_j) + \boldsymbol{\omega}_j$$

where $\boldsymbol{\omega}_j \sim N(0, \mathbf{Q}_j)$ and $\boldsymbol{\Phi}_j = (\partial\boldsymbol{\phi}(\boldsymbol{x})/\partial\boldsymbol{x})|_{(\hat{\boldsymbol{x}}(t_j),\tilde{\mathbf{U}}_j)}$. The INS provides both $\mathbf{Q}_j$ and $\boldsymbol{\Phi}_j$ (see [1, Sec. 7.2.5.2]).

APPENDIX II

This appendix proves Proposition 3.

Proof 6: The linearization error term $\boldsymbol{\epsilon}^i$ is not included in this proof, but can be added by following the idea in the proof of Proposition 2.

The proof first shows the existence of $(\Delta\boldsymbol{p}, \mathbf{N})$ for (43) and (44) and then allows $\boldsymbol{\delta}_2 = 0$ to prove the existence of $(\Delta\boldsymbol{p}, \mathbf{N})$ for (42).

From its definition in Section IV, $\mathcal{Q}_\mathbf{1}$ is a unit column matrix whose column spans the range space of $\mathbf{1} = [1, \ldots, 1]^\mathsf{T} \in \mathbb{R}^K$

$$\mathcal{Q}_\mathbf{1}^\mathsf{T} = [1/\sqrt{K}, \ldots, 1/\sqrt{K}] \in \mathbb{R}^K.$$

Therefore

$$\mathcal{Q}_\mathbf{1}^\mathsf{T} \begin{bmatrix} \bar{H}^i \\ \vdots \\ \bar{H}^i \end{bmatrix} = \sqrt{K}\bar{H}^i \tag{49}$$

for the row vector $\bar{H}^i$ as defined in (35).

Starting from (43), our goal is to show that there exist $\Delta\boldsymbol{p} \in \mathbb{R}^3$ and integer δN^i for $i = 1, \ldots, m$, such that

$$\mathcal{Q}_\mathbf{1}^\mathsf{T}\boldsymbol{h}^i(\hat{\mathbf{X}}_1 \oplus \Delta\boldsymbol{p}) + \lambda\mathcal{R}_\mathbf{1}\big(\hat{N}_1^i + \delta N^i\big) = \mathcal{Q}_\mathbf{1}^\mathsf{T}\boldsymbol{h}^i(\hat{\mathbf{X}}_2) + \lambda\mathcal{R}_\mathbf{1}N_2^i + \mathcal{Q}_\mathbf{1}^\mathsf{T}\boldsymbol{\delta}_2. \tag{50}$$

Let $\delta\mathbf{X} \triangleq \hat{\mathbf{X}}_2 - \hat{\mathbf{X}}_1$ and $\hat{\boldsymbol{p}}_k \in \mathbb{R}^3$ be the position estimates in $\hat{\mathbf{X}}_1$, then

$$\mathcal{Q}_\mathbf{1}^\mathsf{T}\boldsymbol{h}^i(\hat{\mathbf{X}}_2) = \mathcal{Q}_\mathbf{1}^\mathsf{T}\boldsymbol{h}^i(\hat{\mathbf{X}}_1 + \delta\mathbf{X}) \tag{51}$$

$$= \mathcal{Q}_\mathbf{1}^\mathsf{T}\begin{bmatrix} h_1^i(\hat{\boldsymbol{p}}_1 + \Delta\boldsymbol{p}_1) \\ \vdots \\ h_K^i(\hat{\boldsymbol{p}}_K + \Delta\boldsymbol{p}_K) \end{bmatrix} \tag{52}$$

$$= \mathcal{Q}_\mathbf{1}^\mathsf{T}\begin{bmatrix} h_1^i(\hat{\boldsymbol{p}}_1) \\ \vdots \\ h_K^i(\hat{\boldsymbol{p}}_K) \end{bmatrix} + \mathcal{Q}_\mathbf{1}^\mathsf{T}\begin{bmatrix} H_1^i\Delta\boldsymbol{p}_1 \\ \vdots \\ H_K^i\Delta\boldsymbol{p}_K \end{bmatrix} \tag{53}$$

$$= \mathcal{Q}_\mathbf{1}^\mathsf{T}\begin{bmatrix} h_1^i(\hat{\boldsymbol{p}}_1) \\ \vdots \\ h_K^i(\hat{\boldsymbol{p}}_K) \end{bmatrix} + \mathcal{Q}_\mathbf{1}^\mathsf{T}\begin{bmatrix} \bar{H}^i\Delta\boldsymbol{p}_1 \\ \vdots \\ \bar{H}^i\Delta\boldsymbol{p}_K \end{bmatrix} + \mathcal{Q}_\mathbf{1}^\mathsf{T}\begin{bmatrix} \check{H}_1^i\Delta\boldsymbol{p}_1 \\ \vdots \\ \check{H}_K^i\Delta\boldsymbol{p}_K \end{bmatrix} \tag{54}$$

$$= \mathcal{Q}_\mathbf{1}^\mathsf{T}\begin{bmatrix} h_1^i(\hat{\boldsymbol{p}}_1) \\ \vdots \\ h_K^i(\hat{\boldsymbol{p}}_K) \end{bmatrix} + \frac{\bar{H}^i}{\sqrt{K}}\sum_k \Delta\boldsymbol{p}_k + \mathcal{Q}_\mathbf{1}^\mathsf{T}\begin{bmatrix} \check{H}_1^i(\Delta\boldsymbol{p} + \Delta\check{\boldsymbol{p}}_1) \\ \vdots \\ \check{H}_K^i(\Delta\boldsymbol{p} + \Delta\check{\boldsymbol{p}}_K) \end{bmatrix}$$

where $\bar{H}^i$ is the average of Jacobian matrix H_k^i. Define

$$\Delta\boldsymbol{p} = \frac{1}{K}\sum_{i=1}^{K}\Delta\boldsymbol{p}_k \in \mathbb{R}^3 \tag{55}$$

as the average of the position adjustments in $\delta\mathbf{X}$ and $\Delta\check{\boldsymbol{p}}_k = \Delta\boldsymbol{p}_k - \Delta\boldsymbol{p}$ as the variation of the position adjustments.

Continuing, using (55) and then (49) yields

$$\mathcal{Q}_\mathbf{1}^\mathsf{T}\boldsymbol{h}^i(\hat{\mathbf{X}}_2)$$

$$= \mathcal{Q}_\mathbf{1}^\mathsf{T}\begin{bmatrix} h_1^i(\hat{\boldsymbol{p}}_1) \\ \vdots \\ h_K^i(\hat{\boldsymbol{p}}_K) \end{bmatrix} + \sqrt{K}\bar{H}^i\Delta\boldsymbol{p} + \mathcal{Q}_\mathbf{1}^\mathsf{T}\begin{bmatrix} \check{H}_1^i(\Delta\boldsymbol{p} + \Delta\check{\boldsymbol{p}}_1) \\ \vdots \\ \check{H}_K^i(\Delta\boldsymbol{p} + \Delta\check{\boldsymbol{p}}_K) \end{bmatrix}$$

$$= \mathcal{Q}_\mathbf{1}^\mathsf{T}\begin{bmatrix} h_1^i(\hat{\boldsymbol{p}}_1) \\ \vdots \\ h_K^i(\hat{\boldsymbol{p}}_K) \end{bmatrix} + \mathcal{Q}_\mathbf{1}^\mathsf{T}\begin{bmatrix} (\bar{H}^i + \check{H}_1^i)\Delta\boldsymbol{p} \\ \vdots \\ (\bar{H}^i + \check{H}_K^i)\Delta\boldsymbol{p} \end{bmatrix} + \mathcal{Q}_\mathbf{1}^\mathsf{T}\begin{bmatrix} \check{H}_1^i\Delta\check{\boldsymbol{p}}_1 \\ \vdots \\ \check{H}_K^i\Delta\check{\boldsymbol{p}}_K \end{bmatrix}$$

$$= \mathcal{Q}_\mathbf{1}^\mathsf{T}\begin{bmatrix} h_1^i(\hat{\boldsymbol{p}}_1) + H_1^i\Delta\boldsymbol{p} \\ \vdots \\ h_K^i(\hat{\boldsymbol{p}}_K) + H_K^i\Delta\boldsymbol{p} \end{bmatrix} + \mathcal{Q}_\mathbf{1}^\mathsf{T}\begin{bmatrix} \check{H}_1^i\Delta\check{\boldsymbol{p}}_1 \\ \vdots \\ \check{H}_K^i\Delta\check{\boldsymbol{p}}_K \end{bmatrix} \tag{56}$$

$$= \mathcal{Q}_\mathbf{1}^\mathsf{T}\begin{bmatrix} h_1^i(\hat{\boldsymbol{p}}_1 + \Delta\boldsymbol{p}) \\ \vdots \\ h_K^i(\hat{\boldsymbol{p}}_K + \Delta\boldsymbol{p}) \end{bmatrix} + \mathcal{Q}_\mathbf{1}^\mathsf{T}\begin{bmatrix} \check{H}_1^i\Delta\check{\boldsymbol{p}}_1 \\ \vdots \\ \check{H}_K^i\Delta\check{\boldsymbol{p}}_K \end{bmatrix} \tag{57}$$

$$= \mathcal{Q}_\mathbf{1}^\mathsf{T}\boldsymbol{h}^i(\hat{\mathbf{X}}_1 \oplus \Delta\boldsymbol{p}) + \mathcal{Q}_\mathbf{1}^\mathsf{T}\begin{bmatrix} \check{H}_1^i\Delta\check{\boldsymbol{p}}_1 \\ \vdots \\ \check{H}_K^i\Delta\check{\boldsymbol{p}}_K \end{bmatrix}. \tag{58}$$

Thus, with $\hat{N}_1^i + \delta N^i = \hat{N}_2^i$, it follows that:

$$\mathcal{Q}_\mathbf{1}^\mathsf{T}\boldsymbol{h}^i(\hat{\mathbf{X}}_1 \oplus \Delta\boldsymbol{p}) + \lambda\mathcal{R}_\mathbf{1}\big(\hat{N}_1^i + \delta N^i\big) = \mathcal{Q}_\mathbf{1}^\mathsf{T}\boldsymbol{h}^i(\hat{\mathbf{X}}_2) + \lambda\mathcal{R}_\mathbf{1}\hat{N}_2^i + \mathcal{Q}_\mathbf{1}^\mathsf{T}\boldsymbol{\delta}_2$$

where $\boldsymbol{\delta}_2 \triangleq [\check{H}_1^i\Delta\check{\boldsymbol{p}}_1, \ldots, \check{H}_K^i\Delta\check{\boldsymbol{p}}_K]^\mathsf{T}$. With (38), $\|\Delta\check{\boldsymbol{p}}_k\| < \Delta_p$ and $|\epsilon_k^i| < \|\Delta\boldsymbol{p}\|^2/2\underline{\mathrm{D}}$, and the bound in (45) can be derived. This conclusion can also apply to code measurements such that (44) is also valid.

By neglecting the perturbation $\boldsymbol{\delta}_2$ in (43) and (44), (42) can be obtained and this concludes the proof. Note that the definition of $\Delta\boldsymbol{p}$ in (55) is independent of i; therefore, the proof can be repeated for each satellite.

APPENDIX III

This appendix proves Proposition 4. The proof will use the following symbols:

$$\mathbf{X}_1^* = \arg\min_{\mathbf{X}\in\mathbb{R}^{n_s K}} \|\boldsymbol{r}_1(\mathbf{X})\|^2, \quad \mathbf{X}_2^* = \arg\min_{\mathbf{X}\in\mathbb{R}^{n_s K}} \|\boldsymbol{r}_2(\mathbf{X})\|^2$$

$$(\mathbf{X}_\star, \mathbf{N}_\star) \triangleq \arg\min_{\mathbf{X}\in\mathbb{R}^{n_s K}, \mathbf{N}\in\mathbb{Z}^m} \|\boldsymbol{r}_b(\mathbf{X}, \mathbf{N})\|^2$$

and

$$\Delta\boldsymbol{p}_{12}^* = \arg\min_{\Delta\boldsymbol{p}\in\mathbb{R}^3} \big\|\boldsymbol{r}_2\big(\mathbf{X}_1^* \oplus \Delta\boldsymbol{p}\big)\big\|^2.$$

Note that $\mathbf{X}_1^*$, $\mathbf{X}_2^*$, and $\mathbf{X}_\star$ are sets of trajectories. At each time t, with the definition in (3), any trajectory $\mathbf{X}$ can be rewritten as $\mathbf{X} = [\mathbf{P}^\mathsf{T}, \mathbf{S}^\mathsf{T}]^\mathsf{T}$, where $\mathbf{P} = [\mathbf{p}^\mathsf{T}(t_1), \ldots, \boldsymbol{p}^\mathsf{T}(t_K)]^\mathsf{T} \in \mathbb{R}^{3K}$ and $\mathbf{S} = [\mathbf{s}^\mathsf{T}(t_1), \ldots, \boldsymbol{s}^\mathsf{T}(t_K)]^\mathsf{T} \in \mathbb{R}^{K(n_s-3)}$. Because by definition $\|\boldsymbol{r}_2\|^2$ (or $\|\boldsymbol{r}_b\|^2$) is independent of $\mathbf{S}$, the set $\mathbf{X}_2^*$ (or $\mathbf{X}_\star$) contains all trajectories with the same sequence of positions $\mathbf{P}_2^*$, but distinct values of $\mathbf{S}$. Each trajectory in $\mathbf{X}_2^*$ (or $\mathbf{X}_\star$) has the same value for $\|\boldsymbol{r}_2\|^2$ (or $\|\boldsymbol{r}_b\|^2$), but will be penalized differently

by $\|\boldsymbol{r}_1\|^2$. Similarly, $\mathbf{X}_1^*$ is a trajectory set, each having the same shape $\mathbf{S}_1^*$, but with $\mathbf{P}$ shifted by a common vector $\Delta\boldsymbol{p}$ by Proposition 2. Each trajectory in $\mathbf{X}_1^*$ has the same value for $\|\boldsymbol{r}_1\|^2$ but different penalty for $\|\boldsymbol{r}_b\|^2$.

Proof 7: By the definition of $(\mathbf{X}_\star, \mathbf{N}_\star)$, it follows that for the float solution $\check{\mathbf{X}}$ defined in (12), $\forall(\Delta\boldsymbol{p}, \mathbf{N}) \in \mathbb{R}^3 \cup \mathbb{Z}^m$:

$$\|\boldsymbol{r}_b(\mathbf{X}_\star, \mathbf{N}_\star)\|^2 \leq \|\boldsymbol{r}_b(\check{\mathbf{X}} \oplus \Delta\boldsymbol{p}, \mathbf{N})\|^2. \tag{59}$$

Given $(\check{\mathbf{X}}, \check{\mathbf{N}})$ and $(\mathbf{X}_\star, \mathbf{N}_\star)$, the unique $(\Delta\boldsymbol{p}^\star, \mathbf{N}^\star)$ such that

$$\|\boldsymbol{r}_b(\check{\mathbf{X}} \oplus \Delta\boldsymbol{p}^\star, \mathbf{N}^\star)\|^2 = \|\boldsymbol{r}_b(\mathbf{X}_\star, \mathbf{N}_\star)\|^2 \tag{60}$$

is provided in Appendix II in the proof of Proposition 3. From Proposition 2 (with $\boldsymbol{\delta}_1 = \mathbf{0}$), it follows that:

$$\|\boldsymbol{r}_1(\check{\mathbf{X}} \oplus \Delta\boldsymbol{p}^\star)\|^2 = \|\boldsymbol{r}_1(\check{\mathbf{X}})\|^2. \tag{61}$$

Similarly, by Proposition 2 (with $\boldsymbol{\delta}_1 = \mathbf{0}$), it can also be proved that

$$\left\|\boldsymbol{r}_1\left(\mathbf{X}_1^* \oplus \Delta\boldsymbol{p}_{12}^*\right)\right\|^2 = \left\|\boldsymbol{r}_1\left(\mathbf{X}_1^*\right)\right\|^2. \tag{62}$$

By Proposition 3 (with $\boldsymbol{\delta}_2 = \mathbf{0}$) and considering the identical optimality achieved by $\boldsymbol{p}_{12}^*$ and $\mathbf{X}_2^*$, it follows that:

$$\left\|\boldsymbol{r}_2\left(\mathbf{X}_1^* \oplus \Delta\boldsymbol{p}_{12}^*\right)\right\|^2 = \left\|\boldsymbol{r}_2\left(\mathbf{X}_2^*\right)\right\|^2. \tag{63}$$

Since $\check{\mathbf{X}}$ is the float solution such that

$$\|\boldsymbol{r}_a(\check{\mathbf{X}})\|^2 \leq \|\boldsymbol{r}_a(\mathbf{X})\|^2 \quad \forall\mathbf{X} \in \mathbb{R}^{n_s K}$$

we have

$$\begin{aligned}&\|\boldsymbol{r}_1(\check{\mathbf{X}})\|^2 + \|\boldsymbol{r}_2(\check{\mathbf{X}})\|^2 \\ &\quad\leq \left\|\boldsymbol{r}_1\left(\mathbf{X}_1^* \oplus \Delta\boldsymbol{p}_{12}^*\right)\right\|^2 + \left\|\boldsymbol{r}_2\left(\mathbf{X}_1^* \oplus \Delta\boldsymbol{p}_{12}^*\right)\right\|^2.\end{aligned} \tag{64}$$

Substituting (62) and (63) into (64), it follows that:

$$\|\boldsymbol{r}_1(\check{\mathbf{X}})\|^2 + \|\boldsymbol{r}_2(\check{\mathbf{X}})\|^2 \leq \left\|\boldsymbol{r}_1\left(\mathbf{X}_1^*\right)\right\|^2 + \left\|\boldsymbol{r}_2\left(\mathbf{X}_2^*\right)\right\|^2.$$

By the definition of $\mathbf{X}_1^*$ and $\mathbf{X}_2^*$

$$\begin{aligned}\left\|\boldsymbol{r}_1\left(\mathbf{X}_1^*\right)\right\|^2 &\leq \|\boldsymbol{r}_1(\mathbf{X})\|^2 \quad \forall\mathbf{X} \in \mathbb{R}^{n_s K} \\ \left\|\boldsymbol{r}_2\left(\mathbf{X}_2^*\right)\right\|^2 &\leq \|\boldsymbol{r}_2(\mathbf{X})\|^2 \quad \forall\mathbf{X} \in \mathbb{R}^{n_s K}.\end{aligned} \tag{65}$$

Combining these three inequalities yields

$$\|\boldsymbol{r}_1(\check{\mathbf{X}})\|^2 = \left\|\boldsymbol{r}_1\left(\mathbf{X}_1^*\right)\right\|^2. \tag{66}$$

By the definition of $(\mathbf{X}_\star, \mathbf{N}_\star)$, it follows that:

$$\|\boldsymbol{r}_b(\mathbf{X}_\star, \mathbf{N}_\star)\|^2 \leq \|\boldsymbol{r}_b(\mathbf{X}, \mathbf{N})\|^2 \quad \forall(\mathbf{X}, \mathbf{N}) \in \mathbb{R}^{n_s K} \times \mathbb{Z}^m. \tag{67}$$

With (65), (67), and $\|\boldsymbol{r}_1\|^2 + \|\boldsymbol{r}_b\|^2 = \|\boldsymbol{r}\|^2$, it follows that:

$$\left\|\boldsymbol{r}_1\left(\mathbf{X}_1^*\right)\right\|^2 + \|\boldsymbol{r}_b(\mathbf{X}_\star, \mathbf{N}_\star)\|^2 \leq \|\boldsymbol{r}(\mathbf{X}, \mathbf{N})\|^2 \quad \forall(\mathbf{X}, \mathbf{N}).$$

Then, it follows that:

$$\left\|\boldsymbol{r}_1\left(\mathbf{X}_1^*\right)\right\|^2 + \|\boldsymbol{r}_b(\mathbf{X}_\star, \mathbf{N}_\star)\|^2 \leq \|\boldsymbol{r}(\mathbf{X}^*, \mathbf{N}^*)\|^2. \tag{68}$$

From (60), (61), and (66)

$$\|\boldsymbol{r}_1(\check{\mathbf{X}} \oplus \Delta\boldsymbol{p}^\star)\|^2 + \|\boldsymbol{r}_b(\check{\mathbf{X}} \oplus \Delta\boldsymbol{p}^\star, \mathbf{N}^\star)\|^2 \leq \|\boldsymbol{r}(\mathbf{X}^*, \mathbf{N}^*)\|^2 \tag{69}$$

that is

$$\|\boldsymbol{r}(\check{\mathbf{X}} \oplus \Delta\boldsymbol{p}^\star, \mathbf{N}^\star)\|^2 \leq \|\boldsymbol{r}(\mathbf{X}^*, \mathbf{N}^*)\|^2. \tag{70}$$

On the other hand, from (11), we have

$$\|\boldsymbol{r}(\mathbf{X}^*, \mathbf{N}^*)\|^2 \leq \|\boldsymbol{r}(\mathbf{X}, \mathbf{N})\|^2 \quad \forall\mathbf{X} \in \mathbb{R}^{n_s K},\ \mathbf{N} \in \mathbb{Z}^m.$$

Thus, only equality can stand

$$\|\boldsymbol{r}(\check{\mathbf{X}} \oplus \Delta\boldsymbol{p}^\star, \mathbf{N}^\star)\|^2 = \|\boldsymbol{r}(\mathbf{X}^*, \mathbf{N}^*)\|^2$$

and this concludes the proof.

APPENDIX IV

This appendix proves Proposition 5 using similar techniques as were used for proving Proposition 4. In this proof, $\check{\mathbf{X}}$ and $\Delta\boldsymbol{p}^\star$ are known and fixed.

Proof 8: Proposition 1 shows that the float solution $\check{\mathbf{X}}$ is equal to the integer-free solution, which optimizes the cost $\|\boldsymbol{r}_a(\mathbf{X})\|^2$ such that

$$\|\boldsymbol{r}_a(\check{\mathbf{X}})\|^2 \leq \|\boldsymbol{r}_a(\mathbf{X})\|^2 \quad \forall\mathbf{X} \in \mathbb{R}^{n_s K}.$$

Taking the norm of (30) after replacing $\boldsymbol{\delta}_1$ with (41), it follows that:

$$\begin{aligned}&\left\|\bar{\mathcal{Q}}_1^\intercal(\boldsymbol{h}^i(\check{\mathbf{X}} \oplus \Delta\boldsymbol{p}^\star) - \boldsymbol{\varphi}^i)\right\|^2_{\sigma_\varphi^2\mathbf{I}^-} \\ &\quad= \left\|\bar{\mathcal{Q}}_1^\intercal(\boldsymbol{h}^i(\check{\mathbf{X}}) - \boldsymbol{\varphi}^i)\right\|^2_{\sigma_\varphi^2\mathbf{I}^-} \\ &\qquad+2\begin{bmatrix}\check{H}_1^i\Delta\boldsymbol{p}^\star + \epsilon_1^i \\ \vdots \\ \check{H}_K^i\Delta\boldsymbol{p}^\star + \epsilon_K^i\end{bmatrix}^\intercal \bar{\mathcal{Q}}_{\mathbf{1}}(\sigma_\varphi^2\mathbf{I}^-)^{-1}\bar{\mathcal{Q}}_{\mathbf{1}}^\intercal(\boldsymbol{h}^i(\check{\mathbf{X}}) - \boldsymbol{\varphi}^i) \\ &\qquad+\left\|\bar{\mathcal{Q}}_1^\intercal\begin{bmatrix}\check{H}_1^i\Delta\boldsymbol{p}^\star + \epsilon_1^i \\ \vdots \\ \check{H}_K^i\Delta\boldsymbol{p}^\star + \epsilon_K^i\end{bmatrix}\right\|^2_{\sigma_\varphi^2\mathbf{I}^-}.\end{aligned} \tag{71}$$

Given the Gaussian noise assumptions, after convergence of the float solution optimization process, the residual $\bar{\mathcal{Q}}_{\mathbf{1}}^\intercal(\boldsymbol{h}^i(\check{\mathbf{X}}) - \boldsymbol{\varphi}^i)$ is a zero-mean random variable modeled as Gaussian. Therefore, the expected value of (71) yields

$$\begin{aligned}&\boldsymbol{E}\left\{\left\|\bar{\mathcal{Q}}_1^\intercal(\boldsymbol{h}^i(\check{\mathbf{X}} \oplus \Delta\boldsymbol{p}^\star) - \boldsymbol{\varphi}^i)\right\|^2_{\sigma_\varphi^2\mathbf{I}^-}\right\} \\ &\quad\leq \boldsymbol{E}\left\{\left\|\bar{\mathcal{Q}}_1^\intercal(\boldsymbol{h}^i(\check{\mathbf{X}}) - \boldsymbol{\varphi}^i)\right\|^2_{\sigma_\varphi^2\mathbf{I}^-}\right\} + \sigma_\varphi^{-2}K[B_1(\|\Delta\boldsymbol{p}^\star\|, \bar{v})]^2\end{aligned} \tag{72}$$

because $\mathcal{Q} = [\mathcal{Q}_{\mathbf{1}}, \bar{\mathcal{Q}}_{\mathbf{1}}]$ allows that

$$\left\|\bar{\mathcal{Q}}_1^\intercal\begin{bmatrix}\check{H}_1^i\Delta\boldsymbol{p}^\star + \epsilon_1^i \\ \vdots \\ \check{H}_K^i\Delta\boldsymbol{p}^\star + \epsilon_K^i\end{bmatrix}\right\|^2_{\sigma_\varphi^2\mathbf{I}^-} \leq \left\|\mathcal{Q}^\intercal\begin{bmatrix}\check{H}_1^i\Delta\boldsymbol{p}^\star + \epsilon_1^i \\ \vdots \\ \check{H}_K^i\Delta\boldsymbol{p}^\star + \epsilon_K^i\end{bmatrix}\right\|^2_{\sigma_\varphi^2\mathbf{I}}$$

and $|\check{H}_k\Delta\boldsymbol{p}^\star + \epsilon_k^i| \leq B_1(\Delta\boldsymbol{p}^\star, \bar{v})$, for any $k = 1, \ldots, K$. Note that an inequality analogous to inequality (72) also applies to pseudorange measurements

$$\begin{aligned}&\boldsymbol{E}\left\{\left\|\bar{\mathcal{Q}}_1^\intercal(\boldsymbol{h}^i(\check{\mathbf{X}} \oplus \Delta\boldsymbol{p}^\star) - \boldsymbol{\rho}^i)\right\|^2_{\sigma_\rho^2\mathbf{I}^-}\right\} \\ &\quad\leq \boldsymbol{E}\left\{\left\|\bar{\mathcal{Q}}_1^\intercal(\boldsymbol{h}^i(\check{\mathbf{X}}) - \boldsymbol{\rho}^i)\right\|^2_{\sigma_\rho^2\mathbf{I}^-}\right\} + \sigma_\rho^{-2}K[B_1(\|\Delta\boldsymbol{p}^\star\|, \bar{v})]^2.\end{aligned} \tag{73}$$

Since a CPS $\Delta \boldsymbol{p}$ will not cause any variation in the prior cost and the INS cost terms, it follows that:

$$\boldsymbol{E}\{\|\boldsymbol{r}_1(\check{\mathbf{X}} \oplus \Delta \boldsymbol{p}^{\star})\|^2 - \|\boldsymbol{r}_1(\check{\mathbf{X}})\|^2\} \leq m\left(\sigma_\rho^{-2} + \sigma_\varphi^{-2}\right) K[B_1(\|\Delta \boldsymbol{p}^{\star}\|\bar{v})]^2 \quad (74)$$

where m is the number of available satellites.

Similarly, with Proposition 3 and its proof, it can be derived that

$$\boldsymbol{E}\{\|\boldsymbol{r}_b(\check{\mathbf{X}} \oplus \Delta \boldsymbol{p}^{\star}, \mathbf{N}^{\star})\|^2 - \|\boldsymbol{r}_b(\mathbf{X}_{\star}, \mathbf{N}_{\star})\|^2\} \leq m\left(\sigma_\rho^{-2} + \sigma_\varphi^{-2}\right) K[B_1(\|\Delta \boldsymbol{p}^{\star}\|\bar{v})]^2. \quad (75)$$

Similarly by Proposition 2, it can also be proved that

$$\boldsymbol{E}\left\{\left\|\boldsymbol{r}_1\left(\mathbf{X}_1^* \oplus \Delta \boldsymbol{p}_{12}^*\right)\right\|^2 - \left\|\boldsymbol{r}_1\left(\mathbf{X}_1^*\right)\right\|^2\right\} \leq m\left(\sigma_\rho^{-2} + \sigma_\varphi^{-2}\right) K\left[B_1\left(\left\|\Delta \boldsymbol{p}_{12}^*\right\|\bar{v}\right)\right]^2. \quad (76)$$

By Proposition 3

$$\boldsymbol{E}\left\{\left\|\boldsymbol{r}_2\left(\mathbf{X}_1^* \oplus \Delta \boldsymbol{p}_{12}^*\right)\right\|^2 - \left\|\boldsymbol{r}_2\left(\mathbf{X}_2^*\right)\right\|^2\right\} \leq m\sigma_\rho^{-2} K\left[B_1\left(\left\|\Delta \boldsymbol{p}_{12}^*\right\|, \bar{v}\right)\right]^2. \quad (77)$$

Since $\check{\mathbf{X}}$ is the float solution such that

$$\|\boldsymbol{r}_a(\check{\mathbf{X}})\|^2 \leq \|\boldsymbol{r}_a(\mathbf{X})\|^2 \quad \forall \mathbf{X} \in \mathbb{R}^{n_s K}$$

we have

$$\|\boldsymbol{r}_1(\check{\mathbf{X}})\|^2 + \|\boldsymbol{r}_2(\check{\mathbf{X}})\|^2 \leq \left\|\boldsymbol{r}_1\left(\mathbf{X}_1^* \oplus \Delta \boldsymbol{p}_{12}^*\right)\right\|^2 + \left\|\boldsymbol{r}_2\left(\mathbf{X}_1^* \oplus \Delta \boldsymbol{p}_{12}^*\right)\right\|^2. \quad (78)$$

With inequalities (76), (77), and (78), it follows that:

$$\boldsymbol{E}\left\{\|\boldsymbol{r}_1(\check{\mathbf{X}})\|^2 + \|\boldsymbol{r}_2(\check{\mathbf{X}})\|^2 - \left\|\boldsymbol{r}_1\left(\mathbf{X}_1^*\right)\right\|^2 - \left\|\boldsymbol{r}_2\left(\mathbf{X}_2^*\right)\right\|^2\right\} \leq m\left(2\sigma_\rho^{-2} + \sigma_\varphi^{-2}\right) K\left[B_1\left(\left\|\Delta \boldsymbol{p}_{12}^*\right\|, \bar{v}\right)\right]^2.$$

and then

$$\boldsymbol{E}\left\{\|\boldsymbol{r}_1(\check{\mathbf{X}})\|^2 - \left\|\boldsymbol{r}_1\left(\mathbf{X}_1^*\right)\right\|^2\right\} \leq m\left(2\sigma_\rho^{-2} + \sigma_\varphi^{-2}\right) K\left[B_1\left(\left\|\Delta \boldsymbol{p}_{12}^*\right\|, \bar{v}\right)\right]^2 \quad (79)$$

since $\|\boldsymbol{r}_2(\check{\mathbf{X}})\|^2 - \|\boldsymbol{r}_2(\mathbf{X}_2^*)\|^2 \geq 0$ is always true. From inequalities (74) and (79), it follows that:

$$\boldsymbol{E}\left\{\left\|\boldsymbol{r}_1(\check{\mathbf{X}} \oplus \Delta \boldsymbol{p}^{\star})\right\|^2 - \left\|\boldsymbol{r}_1\left(\mathbf{X}_1^*\right)\right\|^2\right\} \leq m\left(3\sigma_\rho^{-2} + 2\sigma_\varphi^{-2}\right) K[B_1(\Delta, \bar{v})]^2$$

where $\Delta \triangleq \max(\|\Delta \boldsymbol{p}^{\star}\|, \|\Delta \boldsymbol{p}_{12}^*\|)$. Along with inequality (75) and the inequality

$$\left\|\boldsymbol{r}_1\left(\mathbf{X}_1^*\right)\right\|^2 + \|\boldsymbol{r}_b(\mathbf{X}_{\star}, \mathbf{N}_{\star})\|^2 \leq \|\boldsymbol{r}(\mathbf{X}^*, \mathbf{N}^*)\|^2$$

it follows that:

$$\begin{aligned}
&\boldsymbol{E}\{\|\boldsymbol{r}(\check{\mathbf{X}} \oplus \Delta \boldsymbol{p}^{\star}, \mathbf{N}^{\star})\|^2\} \\
&\quad = \boldsymbol{E}\{\|\boldsymbol{r}_1(\check{\mathbf{X}} \oplus \Delta \boldsymbol{p}^{\star})\|^2 + \|\boldsymbol{r}_b(\check{\mathbf{X}} \oplus \Delta \boldsymbol{p}^{\star}, \mathbf{N}^{\star})\|^2\} \\
&\quad \leq \boldsymbol{E}\left\{\left\|\boldsymbol{r}_1\left(\mathbf{X}_1^*\right)\right\|^2 + \|\boldsymbol{r}_b(\mathbf{X}_{\star}, \mathbf{N}_{\star})\|^2\right\} \\
&\qquad + m\left(4\sigma_\rho^{-2} + 3\sigma_\varphi^{-2}\right) K[B_1(\Delta, \bar{v})]^2. \quad (80)
\end{aligned}$$

Following the steps from (67) and (68), it yields that:

$$\begin{aligned}
&\boldsymbol{E}\{\|\boldsymbol{r}(\check{\mathbf{X}} \oplus \Delta \boldsymbol{p}^{\star}, \mathbf{N}^{\star})\|^2\} \\
&\quad \leq \boldsymbol{E}\{\|\boldsymbol{r}(\mathbf{X}^*, \mathbf{N}^*)\|^2\} + m\left(4\sigma_\rho^{-2} + 3\sigma_\varphi^{-2}\right) K[B_1(\Delta, \bar{v})]^2 \\
&\quad = \boldsymbol{E}\{\|\boldsymbol{r}(\mathbf{X}^*, \mathbf{N}^*)\|^2\}(1 + C_3)
\end{aligned}$$

where

$$C_3 = \frac{m\left(4\sigma_\rho^{-2} + 3\sigma_\varphi^{-2}\right) K[B_1(\Delta, \bar{v})]^2}{\boldsymbol{E}\{\|\boldsymbol{r}(\mathbf{X}^*, \mathbf{N}^*)\|^2\}}.$$

The optimum $\|\boldsymbol{r}(\mathbf{X}^*, \mathbf{N}^*)\|^2$ is referred as the *a posteriori* variance factor in classical least squares literature [45]. It can be shown that

$$\boldsymbol{E}\{\|\boldsymbol{r}(\mathbf{X}^*, \mathbf{N}^*)\|^2\} = (2K - 1)m - 3$$

where $(2K-1)m - 3 = (n_s K + 2Km - 3) - (n_s K + m)$ is the difference between the total number of measurements and the total dimension of unknown variables, which is also referred as the *degree of freedom*. Thus, it follows that:

$$C_3 = \frac{m\left(4\sigma_\rho^{-2} + 3\sigma_\varphi^{-2}\right) K[B_1(\Delta, \bar{v})]^2}{(2K - 1)m - 3}.$$

Herein, both $\|\Delta \boldsymbol{p}^{\star}\|$ and $\|\Delta \boldsymbol{p}_{12}^*\|$ are upper bounded by Δ_f, so $\Delta \leq \Delta_f$ and this concludes the proof.

ACKNOWLEDGMENT

This research builds on the software of and technical conversations [39]–[44] with A. I. Mourikis and M. Li also of UCR. These technical collaborations are greatly appreciated.

REFERENCES

[1] J. A. Farrell, *Aided Navigation: GPS With High Rate Sensors*. New York, NY, USA: McGraw-Hill, 2008.

[2] *Global Positioning System Standard Positioning Service Performance Standard*, US DoD Positioning, Navigation, and Timing Executive Committee, Washington, DC, USA, 2008.

[3] E. D. Kaplan and C. J. Hegarty, Eds., *Understanding GPS: Principles and Applications*, 2nd ed. Norwood, MA, USA: Artech House, 2006.

[4] R. A. Snay and T. Soler, "Continuously operating reference station (CORS): History, applications, and future enhancements," *J. Surv. Eng.*, vol. 134, no. 4, pp. 95–104, 2008.

[5] G. Pruitt and C. E. Fly, "NDGPS assessment final report," U.S. Dept. Transp., Washington, DC, USA, Tech. Rep. DTFH61-04-D-00002, 2008.

[6] D. Dettmering and G. Weber, "The EUREF NTRIP-broadcaster: Real-time GNSS data for Europe," in *Proc. IGS Workshop*, Bern, Switzerland, 2004, pp. 107–116.

[7] P. de Jonge and C. Tiberius, "The LAMBDA method for integer ambiguity estimation: Implementation aspects," Faculty Geodetic Eng., TUDelft, Delft, The Netherlands, Tech. Rep. 12, 1996.

[8] X.-W. Chang, X. Yang, and T. Zhou, "MLAMBDA: A modified LAMBDA method for integer least-squares estimation," *J. Geodesy*, vol. 79, no. 9, pp. 552–565, 2005.

[9] X.-W. Chang and T. Zhou, "MILES: MATLAB package for solving mixed integer least squares problems," *GPS Solution*, vol. 11, no. 4, pp. 289–294, 2007.

[10] R. Hatch, "The synergism of GPS code and carrier measurements," in *Proc. 3rd Int. Geodetic Symp. Satellite Doppler Positioning*, vol. 2. 1983, pp. 1213–1231.

[11] R. Hatch, "Instantaneous ambiguity resolution," in *Kinematic Systems in Geodesy, Surveying, and Remote Sensing*, vol. 107. New York, NY, USA: Springer Verlag, 1990, pp. 299–308.

[12] T. Takasu and A. Yasuda, "Development of the low-cost RTK-GPS receiver with an open source program package RTKLIB," in *Proc. Int. Symp. GPS/GNSS*, Jeju, Korea, 2009, pp. 1–8.

[13] J. A. Farrell, T. D. Givargis, and M. J. Barth, "Real-time differential carrier phase GPS-aided INS," *IEEE Trans. Control Syst. Technol.*, vol. 8, no. 4, pp. 709–721, Jul. 2000.

[14] S. Zhao, Y. Chen, H. Zhang, and J. A. Farrell, "Differential GPS aided inertial navigation: A contemplative realtime approach," in *Proc. 19th IFAC World Congr.*, Cape Town, South Africa, Aug. 2014, pp. 8959–8964.

[15] Y. Chen, D. Zheng, P. M. Miller, and J. A. Farrell, "Underwater vehicle near real time state estimation," in *Proc. IEEE Int. Conf. Control Appl.*, Hyderabad, India, Aug. 2013, pp. 545–550.
[16] Y. Chen, D. Zheng, P. M. Miller, and J. A. Farrell, "Underwater inertial navigation with long base line transceivers: A near-real-time approach," in *Proc. IEEE 52nd Annu. CDC*, Florence, Italy, Dec. 2013, pp. 5042–5047.
[17] Y. Chen, S. Zhao, D. Zheng, and J. A. Farrell, "High reliability integer ambiguity resolution of 6DOF RTK GPS/INS," in *Proc. IEEE 53rd Annu. CDC*, Los Angeles, CA, USA, Dec. 2014, pp. 6609–6614.
[18] Y. Chen, D. Zheng, P. A. Miller, and J. A. Farrell, "Underwater inertial navigation with long base line transceivers: A near-real-time approach," *IEEE Trans. Control Syst. Technol.*, vol. PP, no. 99, p. 1.
[19] S. Zhao, Y. Chen, and J. A. Farrell, "High precision 6DOF vehicle navigation in urban environments using a low-cost single-frequency GPS receiver," in *Proc. IROS/PPNIV*, Chicago, IL, USA, Sep. 2014, pp. 1–5.
[20] F. Dellaert and M. Kaess, "Square root SAM: Simultaneous localization and mapping via square root information smoothing," *Int. J. Robot. Res.*, vol. 25, no. 12, pp. 1181–1203, 2006.
[21] M. Kaess, A. Ranganathan, and F. Dellaert, "iSAM: Incremental smoothing and mapping," *IEEE Trans. Robot.*, vol. 24, no. 6, pp. 1365–1378, Dec. 2008.
[22] M. Kaess and F. Dellaert, "Covariance recovery from a square root information matrix for data association," *Robot. Auto. Syst.*, vol. 57, no. 12, pp. 1198–1210, 2009.
[23] M. Kaess, H. Johannsson, R. Roberts, V. Ila, J. J. Leonard, and F. Dellaert, "iSAM2: Incremental smoothing and mapping using the Bayes tree," *Int. J. Robot. Res.*, vol. 31, no. 2, pp. 216–235, Feb. 2012.
[24] S. Hewitson, H. K. Lee, and J. Wang, "Localizability analysis for GPS/Galileo receiver autonomous integrity monitoring," *J. Navigat.*, vol. 57, no. 2, pp. 245–259, 2004.
[25] S. Hewitson and J. Wang, "Extended receiver autonomous integrity monitoring (eRAIM) for GNSS/INS integration," *J. Surv. Eng.*, vol. 136, no. 1, pp. 13–22, 2010.
[26] P. Misra and P. Enge, *Global Positioning System: Signals, Measurements and Performance*. Lincoln, MA, USA: Ganga-Jamuna Press, 2001.
[27] S. M. Kay, *Fundamentals of Statistical Signal Processing: Estimation Theory*. Upper Saddle River, NJ, USA: Prentice-Hall, 1993.
[28] X. Chen, F. Dovis, S. Peng, and Y. Morton, "Comparative studies of GPS multipath mitigation methods performance," *IEEE Trans. Aerosp. Electron. Syst.*, vol. 49, no. 3, pp. 1555–1568, Jul. 2013.
[29] P. J. Huber, "Robust estimation of a location parameter," *Ann. Math. Statist.*, vol. 35, no. 1, pp. 73–101, 1964.
[30] D. Wang, H. Lu, and M.-H. Yang, "Least soft-threshold squares tracking," in *Proc. IEEE Conf. CVPR*, Jun. 2013, pp. 2371–2378.
[31] S. Verhagen, "The GNSS integer ambiguities: Estimation and validation," Ph.D. dissertation, Nederlandse Commissie voor Geodesie, Delft, The Netherlands, 2005.
[32] P. J. G. Teunissen, "Least-squares estimation of the integer GPS ambiguities," in *Theory and Methodology*. Beijing, China: IAG, 1993, pp. 1–16.
[33] P. J. G. Teunissen, "The least-squares ambiguity decorrelation adjustment: A method for fast GPS integer ambiguity estimation," *J. Geodesy*, vol. 70, no. 1, pp. 65–82, 1995.
[34] P. J. G. Teunissen, "An optimality property of the integer least-squares estimator," *J. Geodesy*, vol. 73, no. 11, pp. 587–593, 1999.
[35] X.-W. Chang and G. H. Golub, "Solving ellipsoid-constrained integer least squares problems," *SIAM J. Matrix Anal. Appl.*, vol. 31, no. 3, pp. 1071–1089, 2009.
[36] RTCM Special Committee No. 104, *Differential GNSS Services, Version 3*, RTCM Standard 10403.1, Radio Technical Commission for Maritime Services, 2011.
[37] P. Gary and C. E. Fly, *Networked Transport of RTCM via Internet Protocol (NTRIP), Version 2.0*, RTCM Standard 10410.1, Radio Technical Commission for Maritime Services, 2011.
[38] A. Vu, J. A. Farrell, and M. Barth, "Centimeter-accuracy smoothed vehicle trajectory estimation," *IEEE Intell. Transp. Syst. Mag.*, vol. 5, no. 4, pp. 121–135, Winter 2013.
[39] T.-C. Dong-Si and A. I. Mourikis, "Motion tracking with fixed-lag smoothing: Algorithm and consistency analysis," in *Proc. IEEE ICRA*, May 2011, pp. 5655–5662.
[40] M. Li and A. I. Mourikis, "Improving the accuracy of EKF-based visual-inertial odometry," in *Proc. IEEE ICRA*, May 2012, pp. 828–835.
[41] M. Li and A. I. Mourikis, "Vision-aided inertial navigation for resource-constrained systems," in *Proc. IEEE/RSJ Int. Conf. IROS*, Vilamoura, Portugal, Oct. 2012, pp. 1057–1063.
[42] M. Li, B. Kim, and A. I. Mourikis, "Real-time motion estimation on a cellphone using inertial sensing and a rolling-shutter camera," in *Proc. IEEE IROS*, Karlsruhe, Germany, May 2013, pp. 4697–4704.
[43] M. Li, H. Yu, X. Zheng, and A. I. Mourikis, "High-fidelity sensor modeling and self-calibration in vision-aided inertial navigation," in *Proc. IEEE ICRA*, May/Jun. 2014, pp. 409–416.
[44] M. Li and A. I. Mourikis, "High-precision, consistent EKF-based visual–inertial odometry," *Int. J. Robot. Res.*, vol. 32, no. 6, pp. 690–711, May 2013.
[45] E. M. Mikhail and F. E. Ackermann, *Observations and Least Squares*. Lanham, MD, USA: Univ. Press America, 1982.
[46] G. H. Golub and C. F. Van Loan, *Matrix Computations*, 4th ed. Baltimore, MD, USA: The Johns Hopkins Univ. Press, 2012.

Yiming Chen (S'11–M'15) received the B.Eng. degree in automation from Tianjin University, Tianjin, China, in 2009, and the M.S. degrees in electrical engineering and mathematics and the Ph.D. degree in electrical engineering from the University of California at Riverside, Riverside, CA, USA, in 2011, 2013, and 2014, respectively.

He is currently a Senior Engineer with Qualcomm Research, San Diego, CA, USA. His current research interests include sensor fusion, state estimation, optimization, computer vision, machine learning, and automatic control, in particular, their applications in robotics and autonomous vehicles.

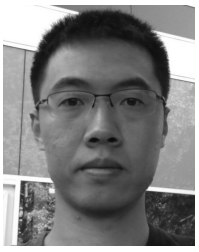

Sheng Zhao received the B.Eng. degree in automation from Xiamen University, Xiamen, China, in 2005, and the Ph.D. degree in electrical engineering from the University of California at Riverside, Riverside, CA, USA, in 2014.

He is currently a Software Engineer with Google, Mountain View, CA, USA. His current research interests include aided inertial navigation systems for robots, autonomous vehicles and mobile devices, state estimation, and simultaneous localization and mapping.

Jay A. Farrell (F'08) received the B.S. degrees in physics and electrical engineering from Iowa State University, Ames, IA, USA, and the M.S. and Ph.D. degrees in electrical engineering from the University of Notre Dame, Notre Dame, IN, USA.

He was with the Draper Laboratory, Cambridge, MA, USA, from 1989 to 1994. He then joined the University of California at Riverside, Riverside, CA, USA, where he is currently a Professor and two time Chair of the Department of Electrical and Computer Engineering. He has authored over 250 technical articles and three books.

Prof. Farrell is a fellow of the American Association for the Advancement of Science and a Distinguished Member of the IEEE Control Systems Society. He has served the IEEE Control Systems Society on their Board of Governors for two terms and served as the Vice President Finance, the Vice President of Technical Activities, the General Chair of the IEEE Conference on Decision and Control in 2012, and the President in 2014.